



# Understanding the interplay between particle shape, grading and sample density on the behaviour of granular assemblies: A DEM approach

Peter Adesina<sup>1,2</sup> · Catherine O'Sullivan<sup>3</sup> · Teng Wang<sup>4</sup>

Received: 4 August 2023 / Accepted: 24 November 2023 / Published online: 5 January 2024  
© The Author(s) 2024

## Abstract

This study investigates the interplay between particle shape, grading and initial sample density, three of the most important factors influencing the mechanical behaviour of sheared granular assemblies. Using the discrete element method (DEM), two-dimensional assemblies of varying initial sample density, particle aspect ratio,  $AR$ , and coefficients of uniformity,  $C_u$ , were prepared and subjected to drained biaxial shearing until the critical state was reached. We assessed the interplay between each of these parameters by evaluating whether the effect of any given parameter on a mechanical quantity is influenced by any other parameter. Our analyses show that the effect of some of these key parameters on mechanical response, can indeed be influenced by other key parameters. The effect of the particle  $AR$  on the peak shear strength for the initially dense assemblies differs when compared with the medium-dense assemblies. The mechanical coordination number of the assemblies at the initial state correlates with the peak strength thereby explaining the interplay between particle  $AR$  and initial sample density on the peak shear strength. The linear relationship established between strength and dilatancy for a combination of all assemblies studied suggests that the strength-dilatancy relationship is a unique characteristic of granular assemblies. The dilatancy of the assemblies correlates strongly with the amount of contacts lost during shearing. The interplays found between particle shape, grading and initial sample density in this study show that to develop robust constitutive models for the prediction of granular material behaviour, the effects of multiple factors must be considered.

**Keywords** DEM · Particle shape · Coefficient of uniformity · Packing density · Biaxial drained shearing

## 1 Introduction

The mechanical behaviour of sands is governed by the interplay between the intrinsic properties such as particle shape, grain size and surface roughness; as well as the extrinsic properties including density, fabric, initial state parameter and stress path. A careful review of the data in the experimental studies on sands supports this conclusion [1–6]. From these experimental studies, it is evident that in order to comprehensively understand the behaviour of sands, it is important to consider multiple determining factors as well as the interplay between them. This is the purpose of the study presented here.

In this study, we seek to understand the interplay between three of the most important factors governing the behaviour of granular assemblies (i.e. particle shape, particle size distribution, and relative density) as acknowledged in the soil mechanics literature. The influence of other important factors (e.g., the initial state parameter

---

✉ Peter Adesina  
p.adesina18@imperial.ac.uk; peter.adesina@inrae.fr;  
greatpetson121@gmail.com

Catherine O'Sullivan  
cath.osullivan@imperial.ac.uk

Teng Wang  
wangteng@connect.hku.hk; wang.teng19@imperial.ac.uk

<sup>1</sup> Dept. of Civil and Environmental Engineering, Imperial College London, South Kensington, London SW7 2AZ, UK

<sup>2</sup> INRAE, UMR RECOVER, Aix-Marseille University, 3275 Rte Cézanne, 40061, 13182 Aix-en-Provence, CS, France

<sup>3</sup> Dept. of Civil and Environmental Engineering, Imperial College London, South Kensington, London SW7 2AZ, UK

<sup>4</sup> Dept. of Civil Engineering, The University of Hong Kong, Pokfulam Road, Hong Kong, Hong Kong

and initial fabric) are beyond the scope of this study. We employ the discrete element method (DEM), a numerical approach which was first proposed by Cundall and Strack [7], for our investigation. DEM allows for a systematic study of the effects of the intrinsic properties of sand, a task that is difficult to achieve in experiments owing to the complex and highly dimensional nature of sand particles. Our motivation for this study stems from the gap identified in the DEM literature where most studies on the mechanical behaviour of granular assemblies have focused on a single influencing factor. Most of the DEM studies that have focused on the effects of particle shape considered only dense assemblies and a single particle size distribution [8–13]. When the effects of particle size distributions were studied using DEM, dense assemblies of discs/spheres were mostly considered [14–17]. With the exception of a small number of DEM studies [18, 19], typically, the effects of initial sample density on the shear behaviour of granular assemblies is studied for a single particle shape [20, 21].

From the earlier experimental and numerical studies where the effect of a single factor is investigated, it is difficult to determine whether the conclusions made are consistent when other factors are considered. Here, we seek to bridge this gap by assessing the interplay between three factors, i.e. particle shape, grading and initial sample density, on the mechanical characteristics of granular assemblies. We assessed whether the effect of a factor  $A$  on a mechanical quantity, at a specific instance of a factor  $B$  varies when the instance changes. For example, we examined whether the effect of particle  $AR$  on the peak  $q/p$  at a specific initial density (controlled by the initial friction coefficient,  $\mu_{prep}$ ), is consistent when the initial density is varied. We also take advantage of the unique capability of DEM to explore the link between the macroscopic characteristics of the granular assemblies studied and their underlying micromechanical features. This is aimed at unravelling the insights that could

help to better understand the interplay between the determining factors and to better interpret laboratory data.

Although three dimensional models allow for a more realistic representation of sands, we conducted our simulations in 2-D as this offers the opportunity to visualise deformation patterns more easily and requires a lower computational effort in comparison to 3-D simulations. While we acknowledge that quantities obtained from 2-D simulations may not directly match those from 3-D models owing to the out-of-plane system response ignored in 2-D, the trends observed in 2-D models agree very well with 3-D models. The data presented in the 2D-DEM study by Adesina et al. [22] supports this claim. In fact, several other experimental and numerical studies have demonstrated that 2-D models of granular materials can adequately capture the complex mechanical phenomena observed in 3-D models and in real granular materials [6, 8, 9, 21, 23–28].

## 2 Numerical simulation approach

The particle shape of focus in this study is the aspect ratio,  $AR$ . Focusing on this single particle shape descriptor allowed us to investigate the interplay between a primary measure of morphology, sample grading and initial packing density simultaneously. We limited consideration to  $AR$  so that the number of required simulations and data generated were manageable. To vary  $AR$  in this study, we adopted a simple approach involving clusters of 2-discs (Fig. 1a). Using this approach, it is not possible to avoid also changing other shape measures and a more detailed consideration of this was given in Adesina et al. [22]; for completeness here we give convexity and sphericity values in Table 1. We acknowledge that more sophisticated approaches such as the use of polygons [13], superquadrics [29, 30] and the level set methods [27], can provide a more realistic representation of particle shape. However, in comparison to the

**Fig. 1** (a) Illustration of particle aspect ratio (b) Particle size distribution for the soil samples with linear grading

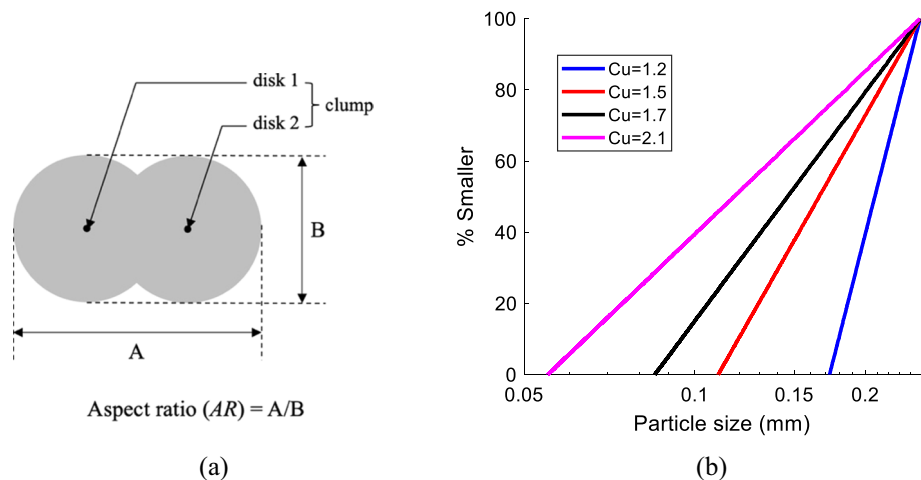


**Table 1** Characteristics of the particles at the different aspect ratios

AR	Sphericity	Convexity	Excluded area(m <sup>2</sup> )
1.0	1.0	1.0	0
1.1	0.9980	0.9994	9.9313e-6
1.2	0.9921	0.9982	2.8671e-5
1.5	0.9515	0.9827	2.3256e-4
1.75	0.8849	0.9488	6.0439e-4
2.0	0.7136	0.8793	1.2670e-3

complex particle modelling approaches, the simple particle shape model adopted here offers an easy contact detection and calculation of contact forces, thereby reducing computational effort [31]. Using clumps of 2-discs to model particle shape does not detract from the behaviour of realistic granular assemblies; indeed, several other researchers who used clumps of 2 or 3 discs/spheres to model non-spherical particles have shown that these simple models yield mechanical behaviour typical of realistic granular assemblies [8–10, 20, 32–36].

The particle AR was varied systematically between 1 and 2. A single disc was used to model AR=1.0 while the distance between the sub-discs in a clump was varied to achieve AR values from 1.1 to 2.0 where  $AR = A/B$  (Fig. 1a). To study the effect of sample grading, the assemblies at each particle AR were generated to have different linear gradings, each with the same maximum particle diameter (A dimension)  $d_{max}=0.25$  mm and different minimum diameter  $d_{min}$  such that the size ratio,  $\lambda = d_{max}/d_{min} = 1.4-4.5$  and  $C_u = d_{60}/d_{10} = 1.2-2.1$  (Fig. 1b), where 60% of the  $d$  (i.e. A dimension) values were smaller than  $d_{60}$  while 10% of the  $d$  values were smaller than  $d_{10}$ . The  $d_{min}$  values are 0.173 mm, 0.11 mm, 0.085 mm and 0.056 mm for  $C_u = 1.2, 1.5, 1.7$  and 2.1, respectively. Although a linear grading can be regarded as an ideal sample grading, using a linear grading and varying the coefficient of uniformity enabled a systematic exploration of the effect of sample grading on the behaviour of granular assemblies.

As shown in Table 2, the number of particles per sample ranged from 5123 for  $C_u = 1.2$  to 22,477 particles at  $C_u = 2.1$ . We increased the sample size as the  $C_u$  increased in order to ensure the samples are statistically representative in

line with [15, 37, 38]. Adesina et al. [39] in their 2-D DEM study on RVE for non-circular particles showed that the granular assemblies generated to have  $C_u = 1.2$  were representative when they contain particles  $\geq 2500$ . The  $C_u$  values considered here were limited to the range  $C_u = 1.2$  to  $C_u = 2.1$  (which indicates the samples are poorly graded) because the computational effort and computer memory required to simulate clusters exceeding 22,477 were prohibitive. The DEM studies that considered particle size distributions wider than those studied here either used a singular sample size (which in most cases is less than 10,000 particles) regardless of  $C_u$  [14, 16, 17, 36, 40] or considered assemblies of spherical particles which require less memory for their simulation in comparison to non-spherical particles [15, 37, 38].

The simulations in this study were conducted using a modified version of LAMMPS [41–43]. Using an in-house algorithm, a non-contacting cloud of particles were generated and enclosed within square periodic boundaries. Isotropic compression of the samples was then performed to a stress state of 100 kPa. Before terminating the isotropic compression, it was ensured that the target stress was achieved and any variation in the coordination number (i.e., the average number of contacts per particle) was less than 0.0001 for at least 500,000 simulation timesteps. To confirm the samples were isotropic, the distribution of contact normal orientations was checked for each sample. The simplified Hertz-Mindlin contact model was used to describe particle interactions in the simulations. The shear modulus,  $G$ , the Poisson’s ratio,  $\nu$ , and the particle density,  $\rho_p$ , used in the simulations were  $27 \times 10^9$  Pa, 0.3 and 2670 kg/m<sup>3</sup>, respectively. During isotropic compression, the packing density of the samples were controlled using the inter-particle friction coefficient ( $\mu_{prep}$ ) such that dense, medium-dense, medium, medium-loose and loose samples used  $\mu_{prep} = 0.01, 0.05, 0.105, 0.2$  and 0.3, respectively. The samples here were not generated to a target relative density as is often the practice in experimental soil mechanics studies. Instead, the sample preparation method adopted here follows the standard practice in DEM studies. While the void ratio,  $e$ , of the dense samples ( $\mu_{prep} = 0.01$ ) here is denoted  $e_{min}$ , the void ratio for the loose samples ( $\mu = 0.3$ ) is denoted  $e_{max}$ ; these  $e_{min}$  and  $e_{max}$  values cannot be mapped directly to  $e_{min}$  and  $e_{max}$  values obtained using standard experimental procedures used in

**Table 2** Summary of simulations completed

Simulation (Effect of sample density and AR)	Number of simulations (Isotropic compression & Shearing)	Sample size (per sample)
$C_u=1.2$ ( $\lambda = 1.4; s = 0.18$ )	60 ( $2 \times 5$ packing densities $\times 6$ AR)	5123 particles
$C_u=1.5$ ( $\lambda = 2.3; s = 0.39$ )	36 ( $2 \times 3$ packing densities $\times 6$ AR)	8795 particles
$C_u=1.7$ ( $\lambda = 2.9; s = 0.49$ )	36 ( $2 \times 3$ packing densities $\times 6$ AR)	12,288 particles
$C_u=2.1$ ( $\lambda = 4.5; s = 0.63$ )	16 ( $2 \times 2$ packing densities $\times 4$ AR)	22,477 particles

$$C_u = d_{60}/d_{10}; \text{ size ratio, } \lambda = d_{max}/d_{min}; \text{ size span, } s = (d_{max} - d_{min}) / (d_{max} + d_{min})$$

soil mechanics. In 2-D, the void ratio is the ratio of the total area of the void space in the periodic cell to the total area of the solid particles. To calculate the area of the particles, the overlap area of the disc in a clump was subtracted from the total area of the discs in the clump.

After isotropic compression, the samples were subjected to strain controlled biaxial compression under a constant confining pressure of  $\sigma_x = 100$  kPa in the  $x$ -direction and a deformation rate in the  $y$ -direction of 0.0005 m/s (Fig. 2). Following the inertial number limit for quasi-static simulations specified by Da Cruz et al. [44], the deformation rate applied here ensured that the simulations were quasi-static as the inertial number for the simulations was less than  $1.02 \times 10^{-5}$ . Although the packing density of the samples were varied using different  $\mu_{prep}$  values, all samples were sheared at  $\mu = 0.3$ . Prior to shearing, the samples generated with  $\mu < 0.3$  were equilibrated using  $\mu = 0.3$  for 10,000,000 timesteps. A total of 148 simulations (74 isotropic compression and 74 biaxial shear) were conducted in this study (Table 2).

### 3 Results

#### 3.1 Initial Packing

At the macroscopic scale, the packing of granular assemblies can be characterised by their void ratio. Figure 3a shows the effect of particle  $AR$  on the initial void ratios,  $e_{min}$  and  $e_{max}$  for the 2-D DEM samples studied here ( $C_u = 1.2$ ) in comparison with the 2-D DEM samples studied by Azéma and Radjaï [8], the 3-D DEM samples studied by Salot et al. [20] and the experimental samples studied by Altuhafi et al. [2]. For the 2-D DEM data studied here, the  $e_{min}$  and  $e_{max}$  initially decreased with an increase in particle  $AR$  until the densest state was reached, and then increased with further increase in  $AR$ . This was the case for all  $C_u$  values studied. This trend agrees with existing data on the effect of  $AR$  on

the packing of granular assemblies in the DEM literature [8, 10, 20, 32, 45, 46]. Figure 3c, d qualitatively illustrate the gap filling efficiencies of the particles with  $AR=1.5$  and  $AR=2.0$ , respectively. The gap filling capability for  $AR = 1.0$  and  $AR= 2.0$  are effectively similar since neither case involve overlapping discs. The initial decrease observed in the  $e_{min}$  and  $e_{max}$  of the granular assemblies as the particle  $AR$  increased from  $AR=1.0$  and  $AR=1.5$  can be attributed to an increase in the gap filling efficiencies of the particles. However, further increase in the particle  $AR$  from  $AR = 1.5$  to  $AR = 2.0$  resulted in a decrease in the gap filling efficiency due to an increase in the excluded particle area (Table 1), hence, the increase in the  $e_{min}$  and  $e_{max}$ .

The  $e_{min}$  and  $e_{max}$  for the natural sand samples in the experimental data by Altuhafi et al. [2] (particle  $AR = 1.26\text{--}1.42$ ) generally increased as  $AR$  increased (Fig. 3a). This increase in void ratio with  $AR$  only occurred when  $AR > 1.5$  in the DEM data presented here and in the DEM literature. It is important to note that the trend observed in the DEM data emerges from a systematically controlled particle shape and covers a range of  $AR$  wider than the  $AR$  for natural sand particles. The particles in natural sand have more complex morphologies and their overall shape differs from the 2-disk clusters considered here. This could explain the variation in the packing of the DEM assemblies in comparison to the experimental samples. Particle shape is difficult to control in experiments.

The  $e_{min}$  and  $e_{max}$  for 2-D DEM samples studied here linearly decreased with an increase in the  $C_u$ , for all  $AR$  considered (Fig. 3b). As the grading of granular assemblies becomes wider, the smaller grains effectively fill the voids within the larger grains. Youd [47] also showed in their experimental study that the  $e_{min}$  and  $e_{max}$  for natural sand increased as the  $C_u$  increased. Similar trends have been reported in the DEM literature on the effect of  $C_u$  on both the initial and the critical state void ratios of granular assemblies [14, 16, 38, 40, 48]. In agreement with the 3-D data

**Fig. 2** Illustration of a sample under biaxial shear

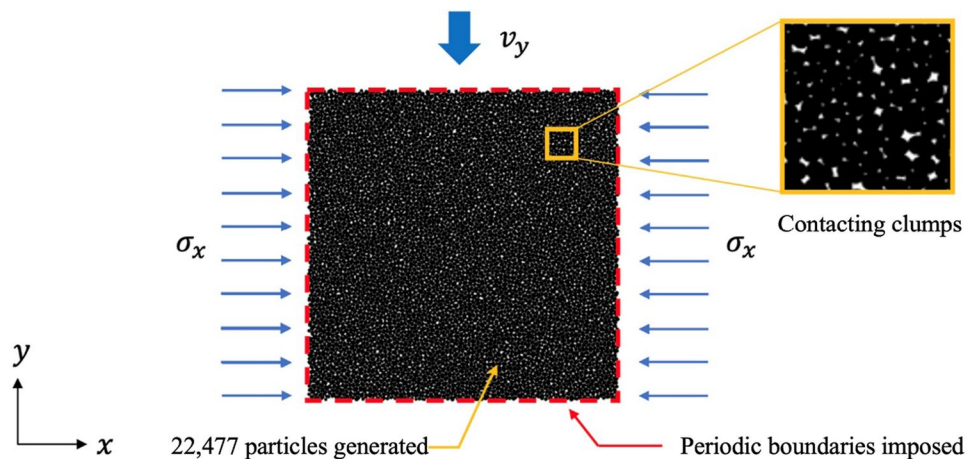
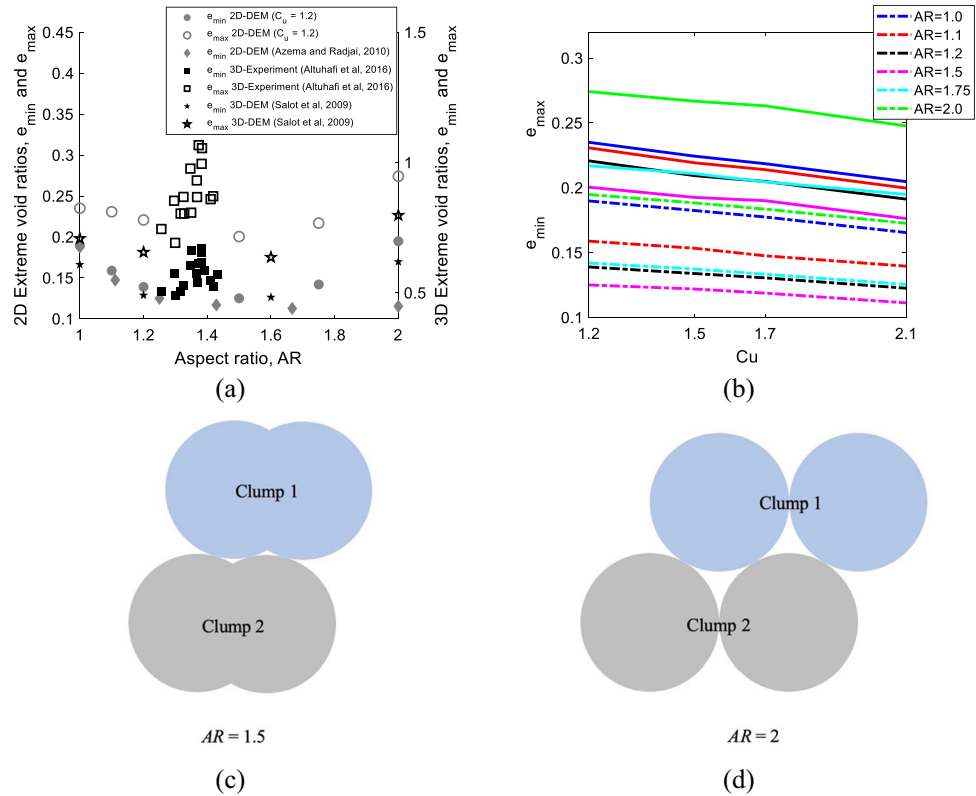


**Fig. 3** Effect of (a)  $AR$  on  $e_{min}$  and  $e_{max}$  for 2D and 3D samples (b)  $C_u$  on  $e_{min}$  (broken lines) and  $e_{max}$  (solid lines). Illustration of gap-filling efficiencies for particle: (c)  $AR=1.5$  (d)  $AR=2.0$  (“2D-DEM  $C_u=1.2$ ” denotes the current study)



in Salot et al. [20], the range of attainable void ratios,  $I_e$ , increased from  $AR = 1.0$  to  $AR=1.2$ , followed by a decrease and an eventual slight increase with further increase in  $AR$  (Fig. 4a).

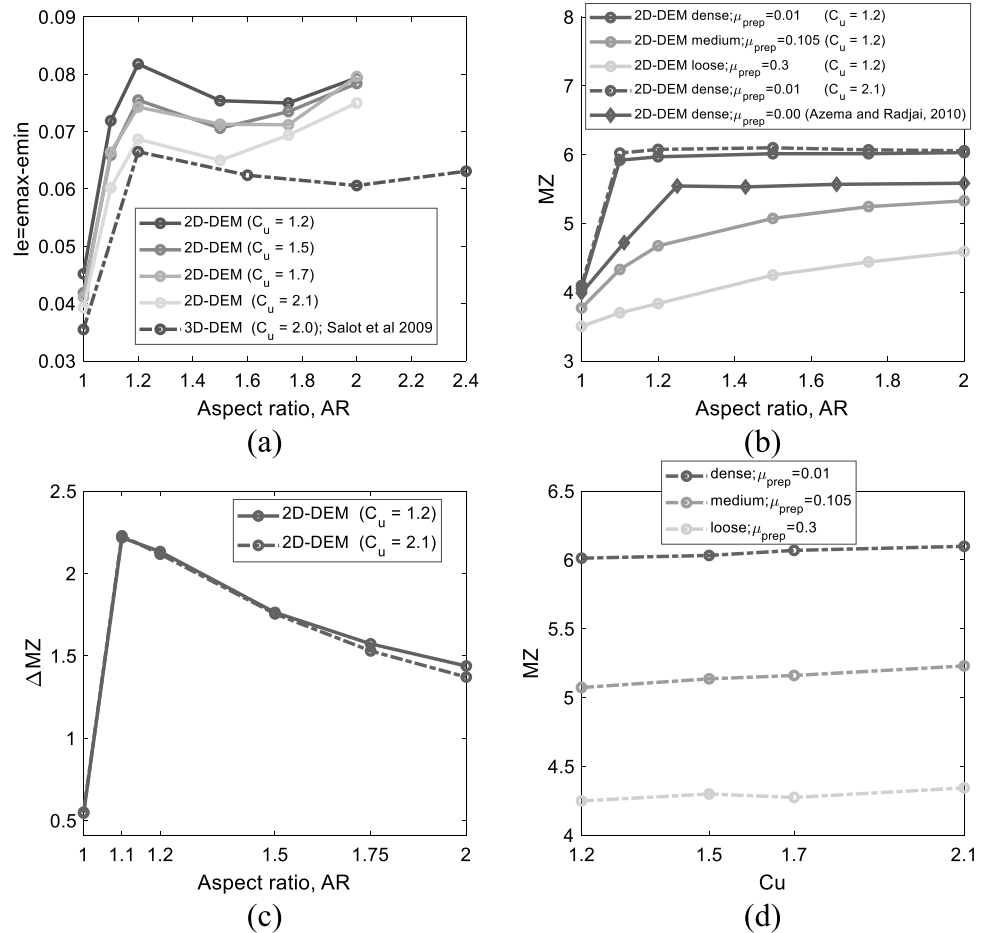
Figure 4b shows the effect of particle  $AR$  on the initial mechanical coordination number,  $MZ$ , of selected granular assemblies studied here, including a comparison with the 2-D DEM data presented by Azéma and Radjaï [8]. The  $MZ$  is the average number of contacts made by particles in a granular assembly when rattlers, i.e., particles with contacts  $\leq 1$ , are excluded. Rattlers do not contribute to stable stress state within granular assemblies [49]. For the initially dense samples ( $\mu_{prep} = 0.01$ ), in agreement with the data presented in Azéma and Radjaï [8], an initial steep increase in the  $MZ$  was observed when particle  $AR$  increased from  $AR = 1.0$  to  $AR = 1.2$  while a further increase in  $AR$  only resulted in a general marginal decrease in the  $MZ$ . The initial  $MZ \approx 4$  found for the near frictionless sample of discs ( $AR = 1.0$ ;  $\mu_{prep} = 0.01$ ) indicates an isostatic state since  $MZ = 2d$ , where  $d$  is the number of degree of freedom per particle [46, 50, 51]. For assemblies of non-circular or non-spherical particles to achieve mechanical equilibrium,  $MZ \leq d(d + 1)$  [8]. The initial  $MZ$  for the medium-dense and the loose samples ( $\mu_{prep} = 0.05$  to  $\mu_{prep} = 0.3$ ) increased with an increase in  $AR$ ; this increase tended to be more linear as  $\mu_{prep}$  increased (Fig. 4b). The difference in the maximum ( $\mu_{prep} = 0.01$ ) and the minimum ( $\mu_{prep} = 0.3$ )  $MZ$  values,  $\Delta MZ_{ini}$ , initially

increased and then declined with further increase in the  $AR$  (Fig. 4c). The initial  $MZ$  increased with an increase in the  $C_u$ , for all sample density considered (Fig. 4d).

### 3.2 Strength and dilatancy

Figure 5 shows the effects of the initial sample densities on the evolution of the stress ratio,  $q/p$ , with axial strain ( $\epsilon_a$ ) and the volumetric strain response for  $C_u = 1.2$  samples having particle  $AR=1.0$ ,  $AR=1.2$  and  $AR=1.5$ . To examine conditions at the critical state, the samples were sheared until  $\epsilon_a \approx 50\%$ . The critical state marks the state at which there is no change in the volume or the void ratio of a sample during shearing. For all the  $AR$  values considered, the  $q/p$  for the initially dense ( $\mu_{prep} = 0.01$ ) and medium-dense samples ( $\mu_{prep} = 0.05$  to  $\mu_{prep} = 0.2$ ) increased to a peak before declining to a plateau at the critical state, where  $q = \sigma_y - \sigma_x$  and  $p = (\sigma_y + \sigma_x)/2$ . As expected, the peak  $q/p$  decreased as the initial density of the samples decreased (i.e. as  $\mu_{prep}$  increased), for all  $AR$  and  $C_u$  values considered. However, the magnitude of the decrease in the peak  $q/p$  as a result of the increase in  $\mu_{prep}$  depends on the  $AR$  (Fig. 7b). This effect which was also reported in the experimental data in Holubec and D’Appolonia [3] and in the DEM data by Ng [18] was found here to correlate with the  $\Delta MZ$  values of the samples ( $\Delta MZ$  was defined in Sect. 3.1). Generally, the higher the

**Fig. 4** Effect of (a) *AR* on the range of attainable void ratios,  $I_e$ , for 2-D and 3-D DEM samples (b) *AR* on the initial *MZ* for 2-D DEM samples (c) *AR* on the difference between the maximum ( $\mu_{prep} = 0.01$ ) and the minimum ( $\mu_{prep} = 0.3$ ) *MZ* values,  $\Delta MZ_{mi}$ , for  $C_u = 1.2$  and  $C_u = 2.1$  samples (d)  $C_u$  on the initial *MZ* for 2-D DEM samples at *AR*=1.5



$\Delta MZ$  value, the greater the effect a change in the  $\mu_{prep}$  had on the peak  $q/p$  (Fig. 7b).

The initially dense and medium-dense samples exhibited a dilative volumetric response (negative  $\epsilon_{vol}$ ), after an initial slight contraction (positive  $\epsilon_{vol}$ ). The dilative volumetric response gradually tended towards a contractive response as the initial sample density decreased (i.e. as  $\mu_{prep}$  increased). The  $q/p$  for the initially loose samples ( $\mu_{prep} = 0.3$ ) increased monotonically until a plateau was reached without a significant softening exhibited. These loose samples generally exhibited a contractive response (positive  $\epsilon_{vol}$ ) during shearing. At the critical state, the  $q/p$  for the samples reached a common value regardless of their initial state. This common  $q/p$  is referred to as the critical state  $q/p$  in classical soil mechanics. The trends observed here are consistent with typical shear strength characteristics of sand obtained from direct shear tests or drained triaxial tests [5, 52–55]. Similar trends were reported in DEM studies where the effect of initial sample density on the shear behaviour of granular assemblies have been studied [20, 21, 26, 56–58].

The effect of particle *AR* on the evolution of the stress ratio,  $q/p$ , and the volumetric strain for the initially dense

( $\mu_{prep} = 0.01$ ), medium-dense ( $\mu_{prep} = 0.105$ ) and loose samples ( $\mu_{prep} = 0.3$ ) having  $Cu = 1.7$  are shown in Fig. 6. For the initially dense samples ( $\mu_{prep} = 0.01$ ), the peak  $q/p$  increased monotonically as *AR* increased from *AR*=1.0 to *AR*=1.5 and then decreased slightly with further increase in the *AR* (Figs. 6a and 7a). This decrease, which is not observed in physical tests on sand, is likely a consequence of the double-disk geometry which occurs when the aspect ratio is high (refer to Fig. 3d). As shown in Fig. 7a, similar trends were reported in the 2-D and the 3-D DEM studies where the effect of *AR* on the peak strength of initially dense assemblies ( $\mu_{prep} = 0.0$ ) were studied [8, 18, 35, 45]. In contrast, the peak  $q/p$  for the medium-dense samples ( $\mu_{prep} = 0.05$  to  $\mu_{prep} = 0.2$ ) increased continually as the particle *AR* increased from *AR*=1.0 to *AR*=2.0, although the increase became marginal at  $AR \geq 1.5$  (Figs. 6b and 7a). Xiao et al. [59] reported similar finding in their experimental study on the effect of particle shape on the stress-dilatancy responses of medium-dense sands. The trend observed here for the peak  $q/p$  is similar to that reported for the initial *MZ* of the samples described in Sect. 3.1 (Fig. 4b).

When the effect of the *AR* on the peak  $q/p$  for the dense assemblies was considered, the *AR* at which the highest

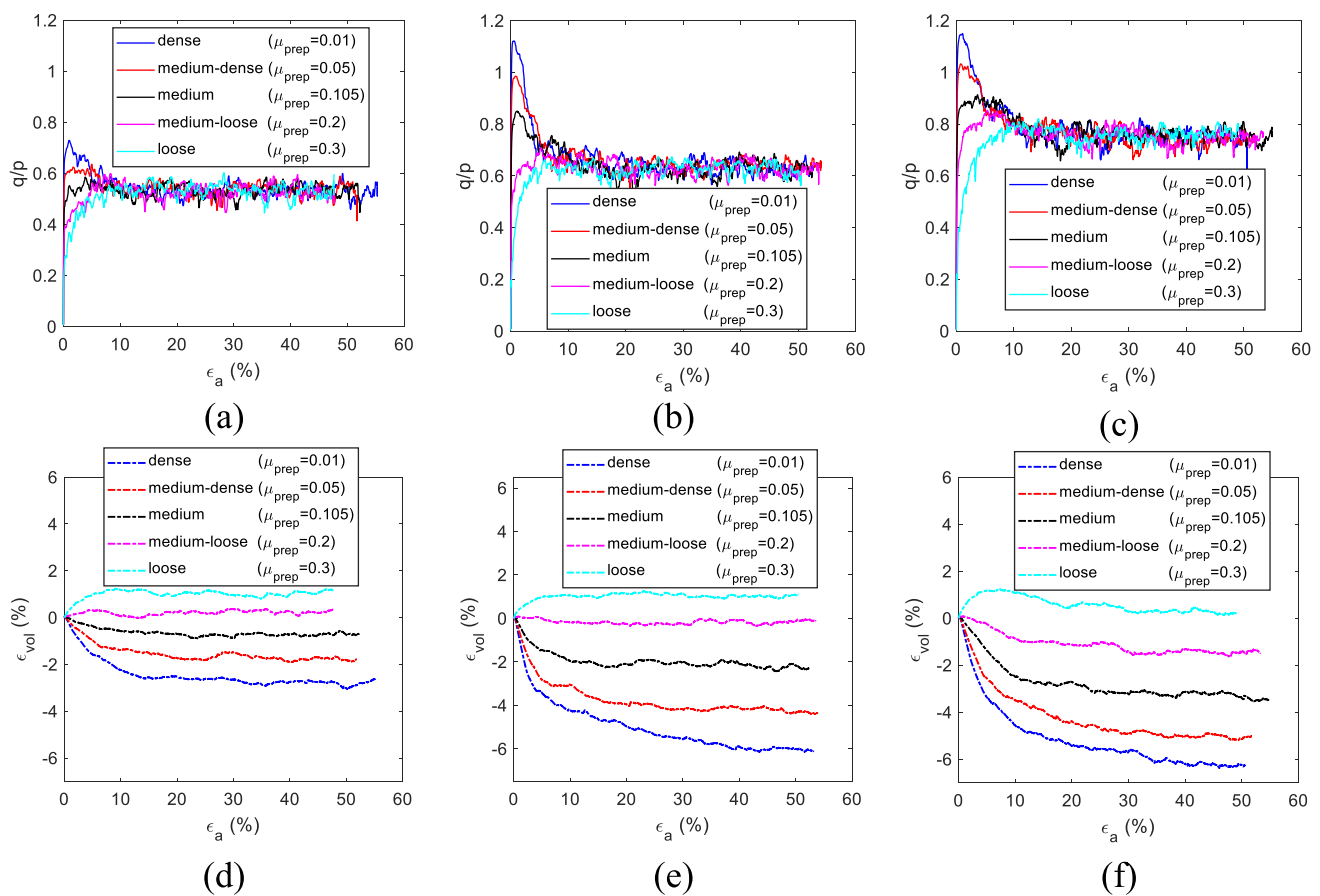


**Fig. 5** Effect of initial sample density ( $\mu_{prep}$ ) on the stress–strain and the volumetric strain responses for  $C_u=1.2$  samples having: (a, d)  $AR=1.0$  (b, e)  $AR=1.2$  (c, f)  $AR=1.5$

peak  $q/p$  was obtained varied with the  $C_u$ . While the highest peak  $q/p$  values for  $C_u = 1.2$  and  $C_u = 1.5$  samples were found at  $AR = 1.5$ , the highest peak  $q/p$  values for  $C_u = 1.7$  and  $C_u = 2.1$  samples were found at  $AR = 1.2$  (Fig. 7c). In agreement with the experimental and the DEM data on the effect of  $AR$  on the strength of granular assemblies [2, 33, 35, 59], the critical state  $q/p$  (i.e., the average  $q/p$  over  $\epsilon_a > 20\%$ ) increased with an increase in the  $AR$ , for all  $C_u$  values considered (Fig. 7d). We observed that the critical state  $q/p$  increased as the  $C_u$  increased for  $AR \leq 1.5$ , however, in agreement with the 2D-DEM data from [9], for  $AR > 1.5$ , the  $C_u$  did not significantly influence the critical state  $q/p$  (Fig. 7e). Jiang et al. [60] in their 3-D DEM study suggested that  $C_u$  has a negligible effect on the critical state strength for the granular assemblies of spherical and non-spherical particles studied.

The volumetric strain for the initially dense ( $\mu_{prep} = 0.01$ ) and the medium-dense samples ( $\mu_{prep} = 0.05$  to  $\mu_{prep} = 0.2$ ) became more dilative as the particle  $AR$  increased, especially at large strains ( $\epsilon_a > 30\%$ ); although the volumetric strains for the samples having  $AR \geq 1.5$  were similar (Fig. 6d, e). This finding agrees with the experimental data presented by

Xiao et al. [59] and the earlier DEM studies which reported the effect of  $AR$  on the volumetric response for dense and medium-dense granular assemblies [6, 10, 13, 33–35, 45]. At  $\epsilon_a \approx 8\%$ , the initially loose samples ( $\mu_{prep} = 0.3$ ) dilated after their initial contraction, before reaching a plateau. While the initial contraction tended to increase with an increase in the  $AR$ ; in the dilative phase (at  $\epsilon_a \geq 8\%$ ), the  $AR$  did not systematically influence the volumetric strain.

Following the strength and dilatancy relationship established for the natural sand of varying particle shapes and  $C_u$  by Bolton [61], we sought to establish a similar relationship for the granular assemblies studied here. The evolution of the dilatancy rate,  $-d\epsilon_v/d\epsilon_a$ , during shearing, for the dense samples ( $\mu_{prep} = 0.01$ ) having  $C_u = 1.2$  (Fig. 8a), is similar to the evolution of the  $q/p$  shown in Fig. 6a; although the peak dilatancy rate,  $(-d\epsilon_v/d\epsilon_a)_{max}$  occurred after the peak  $q/p$ ,  $(q/p)_{max}$  (Fig. 8b). This is in agreement with the data presented by Rothenburg and Bathurst [62] for assemblies of elliptical particles with varying elongations. As the particle  $AR$  increased, the peak dilatancy rate initially increased to a maximum before decreasing with further increase in the  $AR$  (Fig. 8c). In agreement with the experimental data for sand

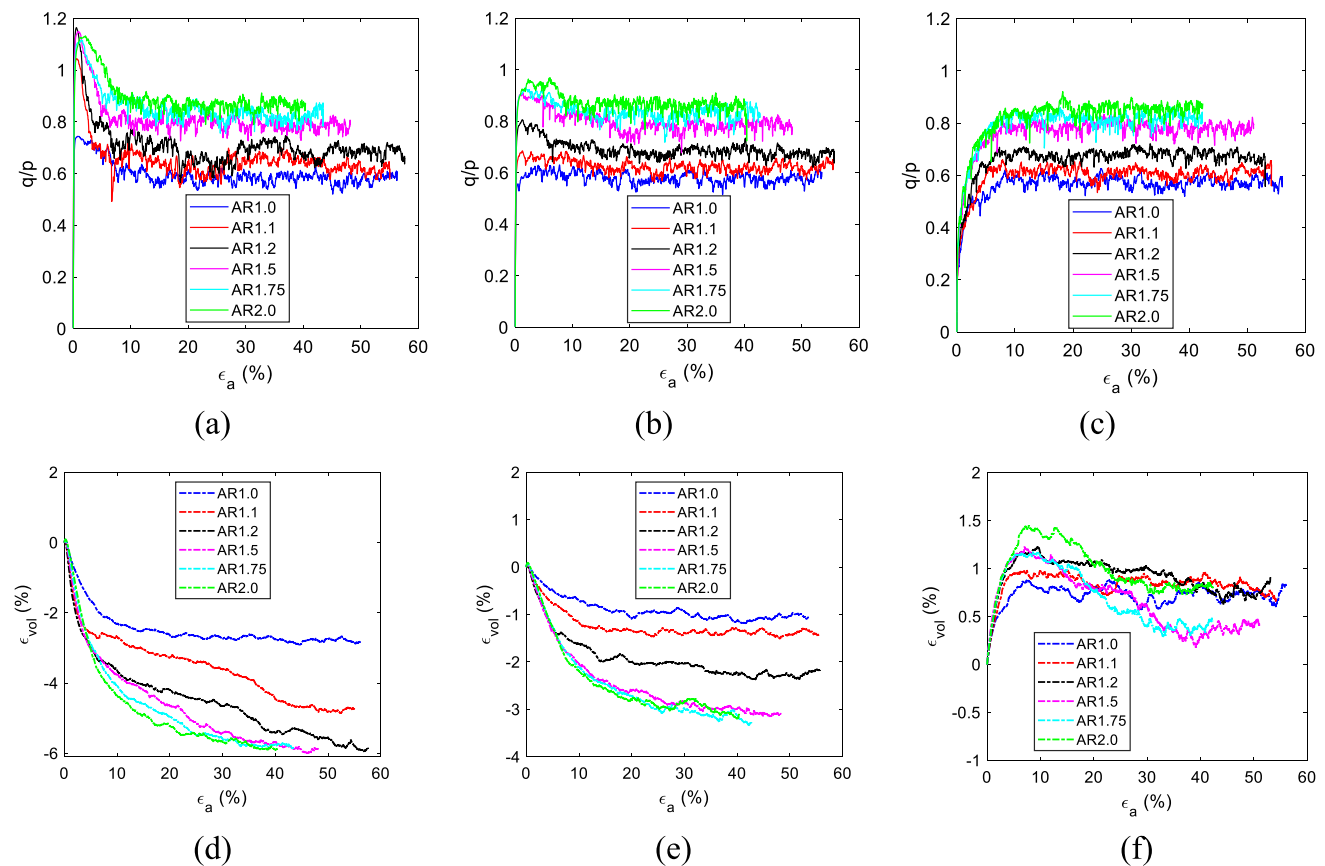


**Fig. 6** Effect of aspect ratio,  $AR$  on the stress–strain responses and the volumetric strain responses for: (a, d) dense ( $\mu_{prep}=0.01$ ); (b, e) medium ( $\mu_{prep}=0.105$ ) (c, f) loose ( $\mu_{prep}=0.3$ ) samples having  $C_u=1.7$

subjected to shearing in plane strain by Bolton [61], a linear relationship was established between the strength and the dilatancy of the granular assemblies of the varying particle  $AR$  and the  $C_u$  values studied here (Fig. 8d).

### 3.3 Critical state void ratio

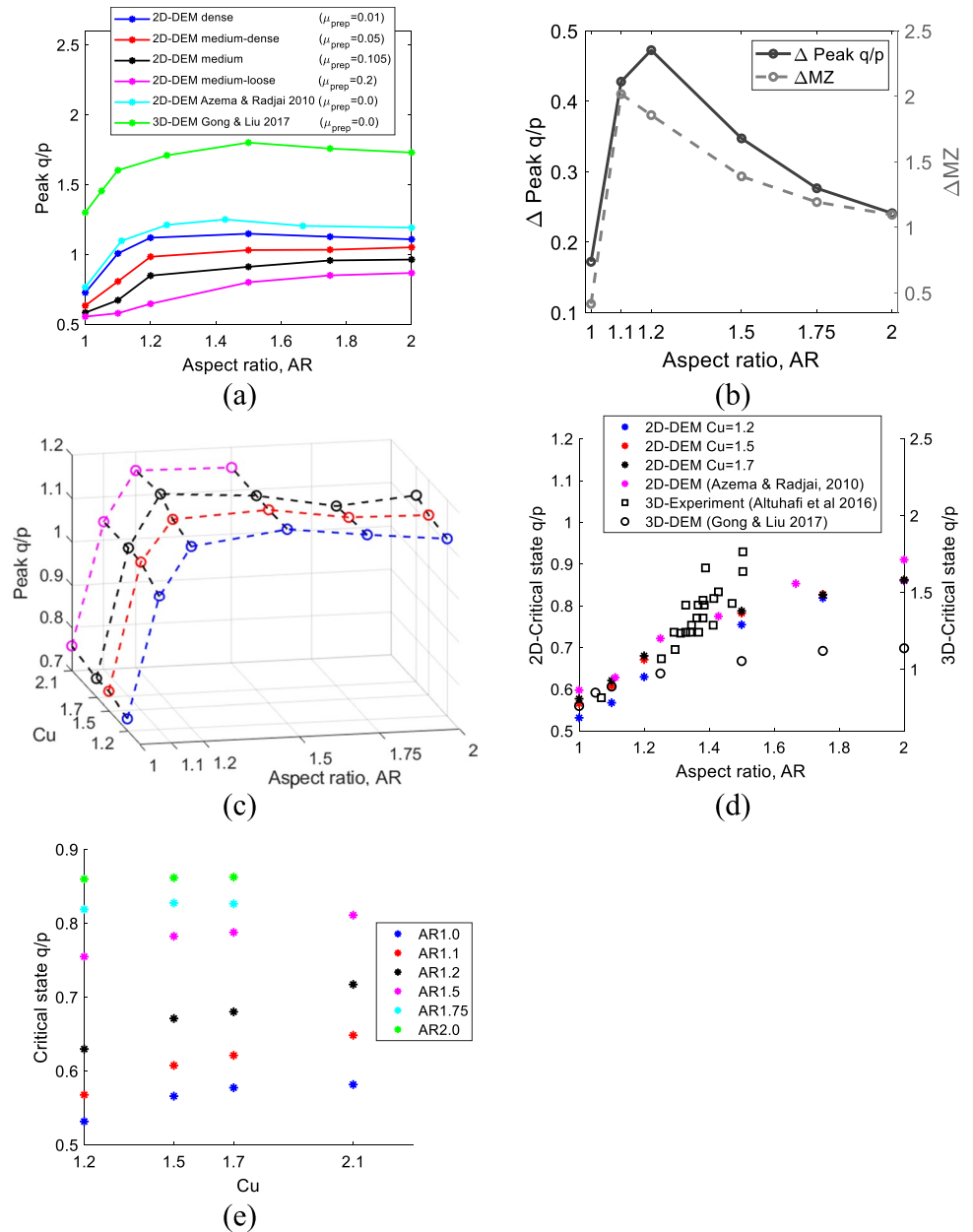
In agreement with earlier experimental studies on sand, the void ratios for the samples of varying initial density studied here converged at large strains during shearing (Fig. 9a). This unique void ratio,  $e$ , is referred to as the critical state void ratio in classic soil mechanics. The effect of the particle  $AR$  on the critical state  $e$  (Fig. 9b) is similar to the observation made after isotropic compression as shown in Fig. 3a. We found for the samples studied here that an increase in the critical state  $q/p$  was not always accompanied by a decrease in the critical state  $e$ . While the critical state  $q/p$  for the samples studied here increased continuously with the  $AR$ , the critical state  $e$  decreased to a minimum and later increased as the  $AR$  increased (Fig. 9c). In agreement with earlier experimental studies, we found that the critical state  $e$  for the samples studied here decreased with an increase in the  $C_u$  values (Fig. 9d).

### 3.4 Contact evolution during shearing

Figure 10a shows the effect of the initial sample density on the evolution of the mechanical coordination number,  $MZ$ , for  $C_u=1.2$  samples having  $AR=1.5$ . In agreement with earlier experimental and DEM studies on granular assemblies [33, 51, 54, 63], the  $MZ$  for the dense ( $\mu_{prep} = 0.01$ ) and the medium-dense samples ( $\mu_{prep} = 0.05$  to  $\mu_{prep} = 0.2$ ) drastically declined until a plateau was reached. An ultimate increase in the  $MZ$  was observed for the initially loose samples ( $\mu_{prep} = 0.3$ ). At the critical state (i.e., at  $\epsilon_a > 20\%$ ), a unique  $MZ$  was attained by the samples irrespective of their initial densities. The percentage of contact loss by the dense samples (measured here as:  $(MZ_{ini} - MZ_{crit})/MZ_{ini} \times 100\%$ , where  $MZ_{ini}$  and  $MZ_{crit}$  are the initial  $MZ$  and the critical state  $MZ$ , respectively), initially increased to a maximum with an increase in the particle  $AR$  before declining with further increase in the  $AR$  (Fig. 10b). A similar trend was observed for the degree of strain softening exhibited by the granular assemblies during shearing, such that a linear relationship was established between the contact loss and the degree of strain softening exhibited by the assemblies (Fig. 10c). The strain softening is measured here



**Fig. 7** Effect of aspect ratio,  $AR$  on the: (a) peak  $q/p$  for 2D and 3D samples at different initial sample density ( $\mu_{prep}$ ) (b)  $\Delta Peak q/p$  (left-side of plot) and  $\Delta MZ$  (right-side of plot), i.e. the difference between the maximum ( $\mu_{prep} = 0.01$ ) and the minimum ( $\mu_{prep} = 0.2$ ) peak  $q/p$  and  $MZ$  values (c) peak  $q/p$  for 2D dense samples ( $\mu_{prep} = 0.01$ ) at different  $C_u$  values ( $C_u = 2.1$  samples which contained 22,477 clump particles were not sheared for  $AR > 1.5$ ) due to the computational effort and computer memory required (d) critical state  $q/p$  for 2D and 3D samples (e) Effect of  $C_u$  on critical state  $q/p$  for samples at different particle  $AR$ . (“2D-DEM  $C_u = 1.2-1.7$ ” denotes the current study)

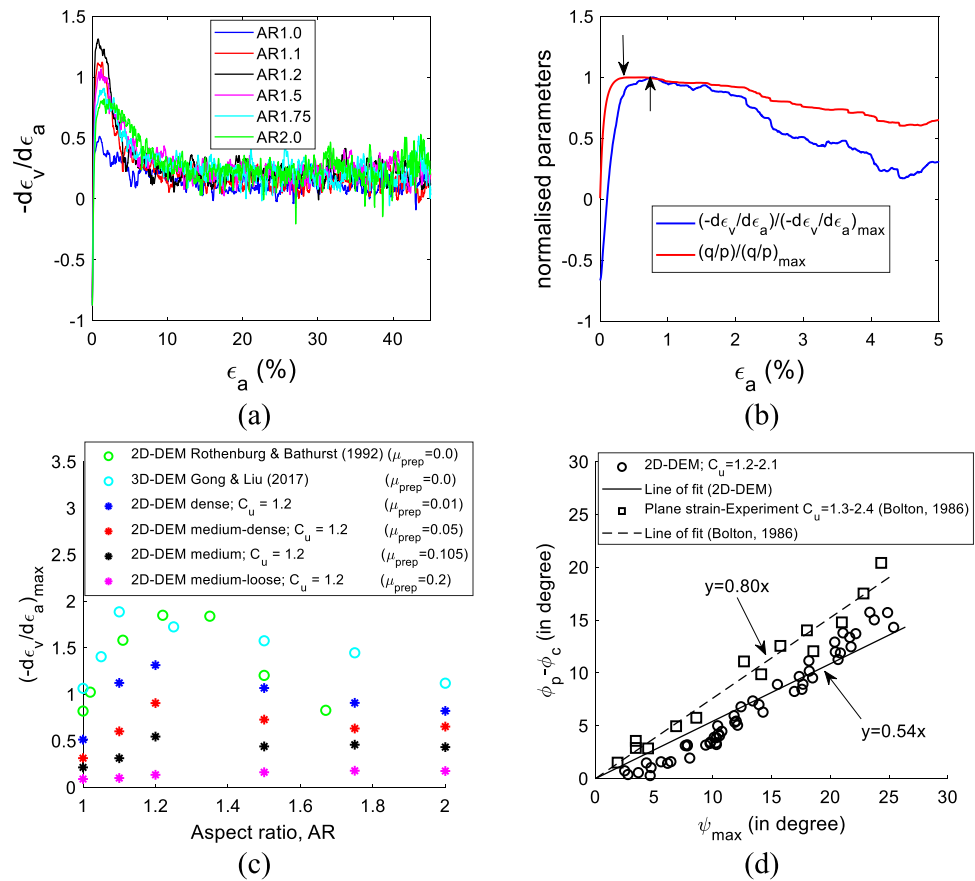


as:  $[(q/p)_{max} - (q/p)_{crit}] / (q/p)_{max} \times 100\%$ , where  $(q/p)_{max}$  and  $(q/p)_{crit}$  are the peak  $q/p$  and the critical state  $q/p$ , respectively. The percentage of contact loss during shearing by the dense granular assemblies also correlates strongly ( $R^2=0.94$ ) with their dilatancy (Fig. 10d). It has been earlier suggested in experimental studies on sand and in DEM studies that dense granular assemblies respond to shearing by losing contacts in addition to a simultaneous breaking of the interlock between particles [4, 13, 33, 51, 52, 64]. The correlation established here between the contact loss and the dilatancy provides a quantitative evidence for this claim.

Again in agreement with earlier experimental and DEM data [8, 13, 45, 54, 62], the critical state  $MZ$  increased with an increase in the particle  $AR$  (Fig. 11a), for all sample densities

and  $C_u$  values considered. The higher the particle  $AR$ , the higher the proportion of the contacts  $\geq 5$  and the lower the proportion of contacts  $\leq 4$  within the granular assemblies (Fig. 11b). This explains the increase in the critical state  $MZ$  as the particle  $AR$  increased. The critical state  $MZ$  increased linearly with an increase in the  $C_u$ , for all  $AR$  considered, although the increase tended to be marginal for  $AR = 1.75$  and  $AR = 2.0$  (Fig. 11c). The average contacts (i.e. the  $MZ$ ) made by the particles within granular assemblies is important since it determines the strength mobilised by the granular assemblies [11, 18, 20, 33]. This is evident in the strong correlation ( $R^2 = 0.96$ ) established between the initial  $MZ$  and the peak strength for the samples of varying particle  $AR$  and  $C_u$  studied here (Fig. 12a). A similar correlation ( $R^2=0.97$ ) was

**Fig. 8** (a) Effect of AR on the evolution of the dilatancy rate,  $-d\epsilon_v/d\epsilon_a$ , during shearing for  $C_u=1.2$  dense samples ( $\mu_{prep}=0.01$ ) (b) Location of maxima for the mobilised  $q/p$  and the  $-d\epsilon_v/d\epsilon_a$  for dense samples ( $\mu_{prep}=0.01$ ) having  $C_u=1.2$  and  $AR=1.2$  (c) Effect of AR and initial sample density,  $\mu_{prep}$ , on the  $(-d\epsilon_v/d\epsilon_a)_{max}$  for 2D and 3D-DEM samples (d) Excess friction angle versus peak dilatancy angle,  $\psi_{max}$  for 2D-DEM and 3D-Experiment samples in plane-strain. (“2D-DEM  $C_u=1.2-2.1$ ” denotes the current study)



established between the critical state  $MZ$  and the critical state  $q/p$  of the assemblies (Fig. 12b).

### 3.5 Fabric anisotropy

The effects of initial sample density, particle AR, and  $C_u$  on the fabric of the granular assemblies studied here were evaluated by determining the particle orientation anisotropy,  $a_p$  and the contact normal orientation anisotropy,  $a_{cn}$  of the assemblies. A second order particle orientation fabric tensor ( $\Phi_{pij}$ ) defined by Satake [65] was calculated as:

$$\Phi_{pij} = \frac{1}{N_p} \sum_{p=1}^{N_p} n_{pi}^p n_{pj}^p \quad (1)$$

where  $N_p$  is the total number of particles in the system and the vector  $n_p$  gives the particle orientation.

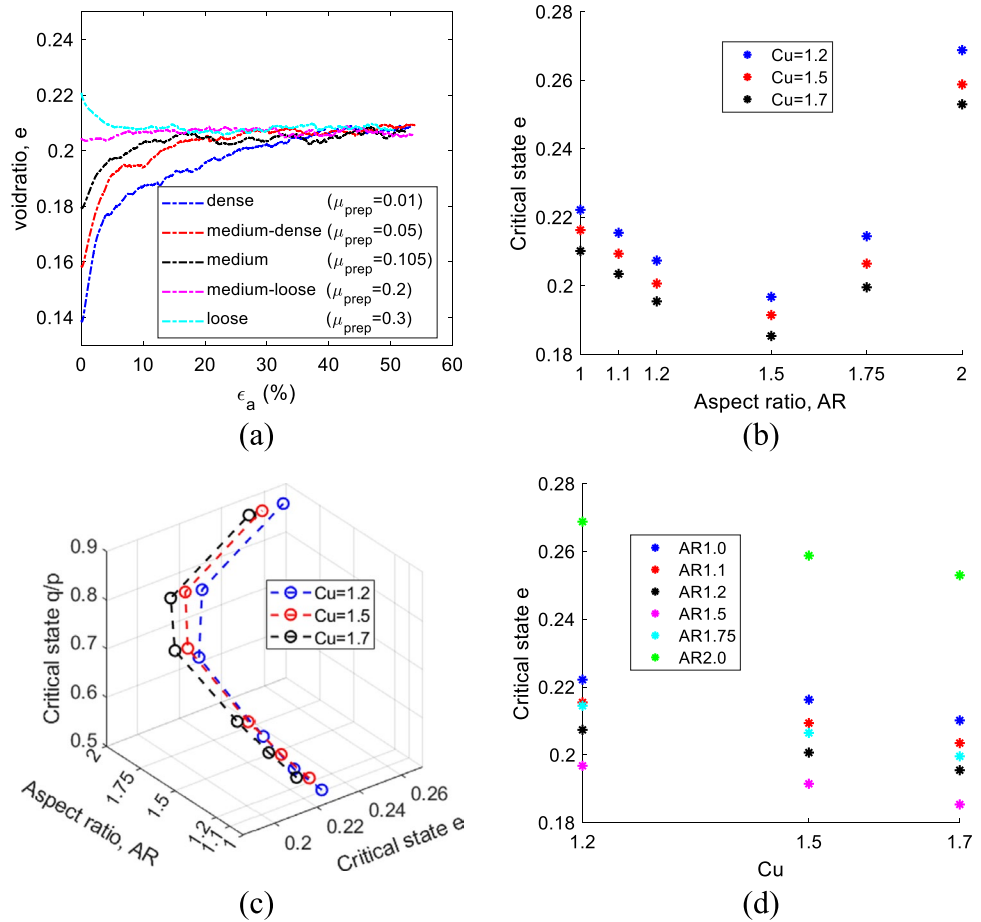
Similarly, the second order contact normal orientation tensor was calculated as:

$$\Phi_{cij} = \frac{1}{N_c} \sum_{c=1}^{N_c} n_{ci}^c n_{cj}^c \quad (2)$$

where  $N_c$  is the total number of contacts in the system and the vector  $n_c$  gives the contact normal orientation. The

fabric anisotropy is quantified as the difference between the major and minor eigenvalues, i.e.,  $a_{cn} = \Phi_{c1} - \Phi_{c2}$  or  $a_p = \Phi_{p1} - \Phi_{p2}$ . A fabric anisotropy value of 0 indicates a perfect isotropic packing. Figure 13a shows the evolution of the  $a_p$  for the initially dense samples having  $C_u = 1.2$ . The  $a_p$  increased continuously and non-linearly as the shearing of the granular assemblies progressed, for all particle AR and sample density considered. While the particle AR did not systematically influence the  $a_p$  after isotropic compression (i.e. at  $\epsilon_a = 0$ ), during shearing, particle AR significantly influenced the  $a_p$  (Fig. 13b). For  $\epsilon_a \leq 20\%$ , the  $a_p$  initially increased to a maximum as the AR increased and then declined with further increase in the AR; while for  $\epsilon_a \geq 30\%$ , a monotonic increase in the  $a_p$  was observed as the particle AR increased. This trend was consistent for all sample densities and the  $C_u$  values studied here. Figure 14 illustrates the effect of the particle AR on the critical state  $a_p$  by comparing the orientations of the particles within the dense granular assemblies having  $AR = 1.1$  and  $AR = 1.5$ . A more pronounced variations in the particle orientations (i.e. lower anisotropy) were observed for  $AR=1.1$  (Fig. 14a) in comparison to  $AR=1.5$  (Fig. 14b) in which the particles were preferentially oriented towards the horizontal as most of the particles had orientations within  $-20^\circ$  and  $+20^\circ$  to the horizontal.

**Fig. 9** (a) Determination of the  $\epsilon_a$  for the critical state  $e$  for  $C_u = 1.2$  samples having  $AR=1.2$  (b) Effect of  $AR$  on the critical state  $e$  at different  $C_u$  values (c) Critical state  $q/p$  plotted against critical state  $e$  at different  $C_u$  values (d) Effect of  $C_u$  on the critical state  $e$  for samples at different particle  $AR$



The effect of the particle  $AR$  on the evolution of the  $a_{cn}$  for the initially dense ( $\mu_{prep} = 0.01$ ) and the initially loose ( $\mu_{prep} = 0.3$ ) samples having  $C_u = 1.2$  are shown in Fig. 13c, d, respectively. In agreement with earlier DEM studies that evaluated the contact normal fabric anisotropy of granular assemblies [34, 51, 57, 63], the evolution of the  $a_{cn}$  echoes a similar trend to that observed for the  $q/p$  (Fig. 6a, c). For the samples having particle  $AR \geq 1.5$ , the  $a_{cn}$  continued to increase until  $\epsilon_a \approx 40\%$  indicating their contact fabric continued to evolve until very large strains (Fig. 13c, d).

While the critical state  $q/p$  increased as the particle  $AR$  increased from  $AR = 1.0$  to  $2.0$  (Fig. 7d), the critical state  $a_{cn}$  increased to a maximum at  $AR = 1.75$  and then decreased with further increase in the  $AR$ , for all  $C_u$  values considered (Fig. 15a). We found that an increase in the critical state  $q/p$  was not always accompanied by an increase in the critical state  $a_{cn}$  (Fig. 15b), especially for  $AR \geq 1.75$ . Similarly, the critical state  $a_{cn}$  does not always increase with the critical state  $MZ$  (Fig. 15c). A similar conclusion could be made from the data in the 2D-DEM study by Azéma and Radjai [8] where the critical state branch vector anisotropy, increased to a maximum and then decreased as particle elongation increased, despite a continuous increase in the critical

state  $MZ$ . In contrast, Azéma and Radjai [8] and Yang et al. [35] reported a continuous increase in the critical state  $a_{cn}$  even for  $AR \geq 2.0$ . As a consequence of the particles taking a preferential orientation towards the horizontal during shearing, the contact normals were preferentially oriented towards the vertical (i.e., parallel to the direction of the major principal stress). This is in agreement with earlier DEM studies on particle shape effect [57, 63].

### 3.6 Particle rotation

The rotation of particles within a granular assembly during shearing could reveal the microscopic mechanisms ensuing within the assembly. In fact, the mobilisation of shear strength by granular assemblies has been associated with their resistance to particle rotation or the lack thereof [4, 6, 20, 27, 66]. Here, we computed particle rotation as the change in particle orientation from the start of shearing (i.e., at  $\epsilon_a = 0\%$ ) to the  $\epsilon_a$  of concern. The mean particle rotation decreased with an increase in the particle  $AR$ , for all sample densities considered. This indicates that particle interlock increased with particle  $AR$ . This trend is consistent whether near the start of shearing (i.e., at

**Fig. 10** (a) Effect of the initial density on the evolution of the mechanical coordination number,  $MZ$ , for  $C_u=1.2$  samples having  $AR=1.5$  (b) Effect of density and  $AR$  on the percentage of contact loss by  $C_u=1.2$  samples. Relationship between (c) the degree of strain softening and the contact loss (d) the peak dilatancy angle,  $\psi_{max}$ , and contact loss during shearing by 2D-DEM samples. (“2D-DEM  $C_u=1.2-2.1$ ” denotes the current study)

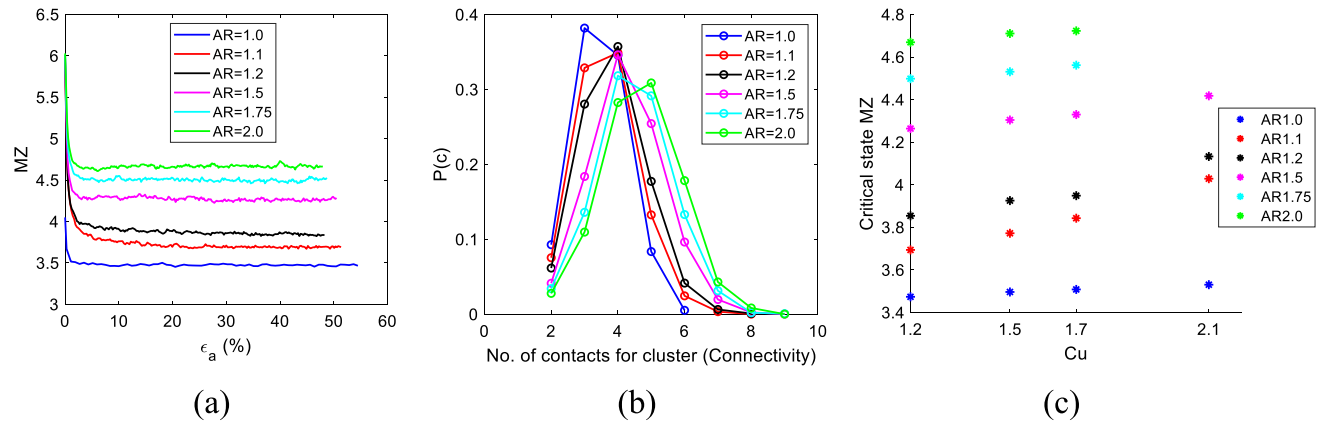
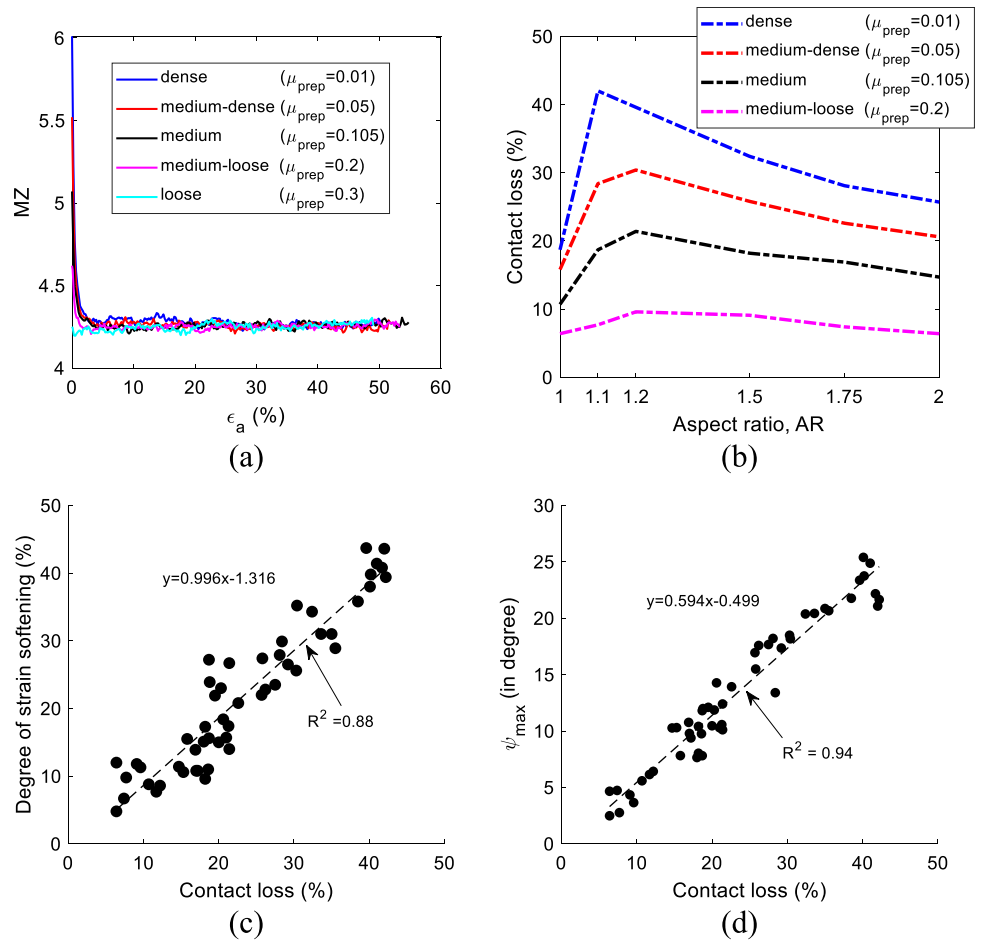


**Fig. 11** (a) Effect of  $AR$  on the evolution of the  $MZ$  for dense ( $\mu_{prep} = 0.01$ ) samples having  $C_u = 1.2$  (b) Connectivity distribution showing the fraction  $P(c)$  of particles with certain connectivity

values at the critical state for the dense ( $\mu_{prep} = 0.01$ ) samples having  $C_u = 1.2$  and  $AR=1.2$  (d) Effect of  $C_u$  on the critical state  $MZ$  for 2D-DEM samples

$\epsilon_a = 1\%$ ; Fig. 16a) or at the critical state (i.e., at  $\epsilon_a = 40\%$ ; Fig. 16b). The looser the initial state of the samples, the higher the mean particle rotation. Looser packings generally have more room for particle rotation while particle rotation is frustrated in dense packings [4, 54]. The

decrease in particle rotation associated with increasing  $AR$  could explain the increase observed in the critical state  $q/p$  when particle  $AR$  was increased as shown in Fig. 7d. In the literature, the shear strength mobilised by granular assemblies of non-spherical particles has been attributed

**Fig. 12** (a) Relationship between peak  $q/p$  and  $MZ$  after isotropic compression (b) Relationship between critical state  $q/p$  and critical state  $MZ$  for 2D-DEM samples

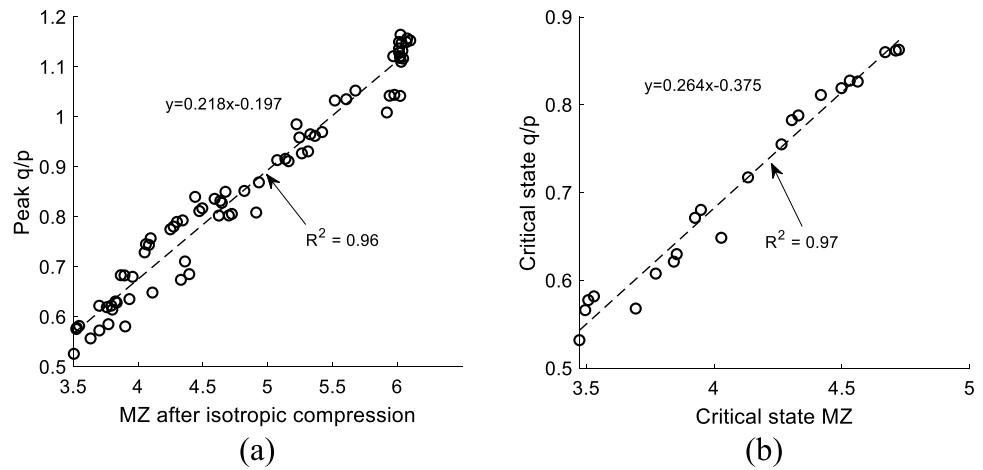
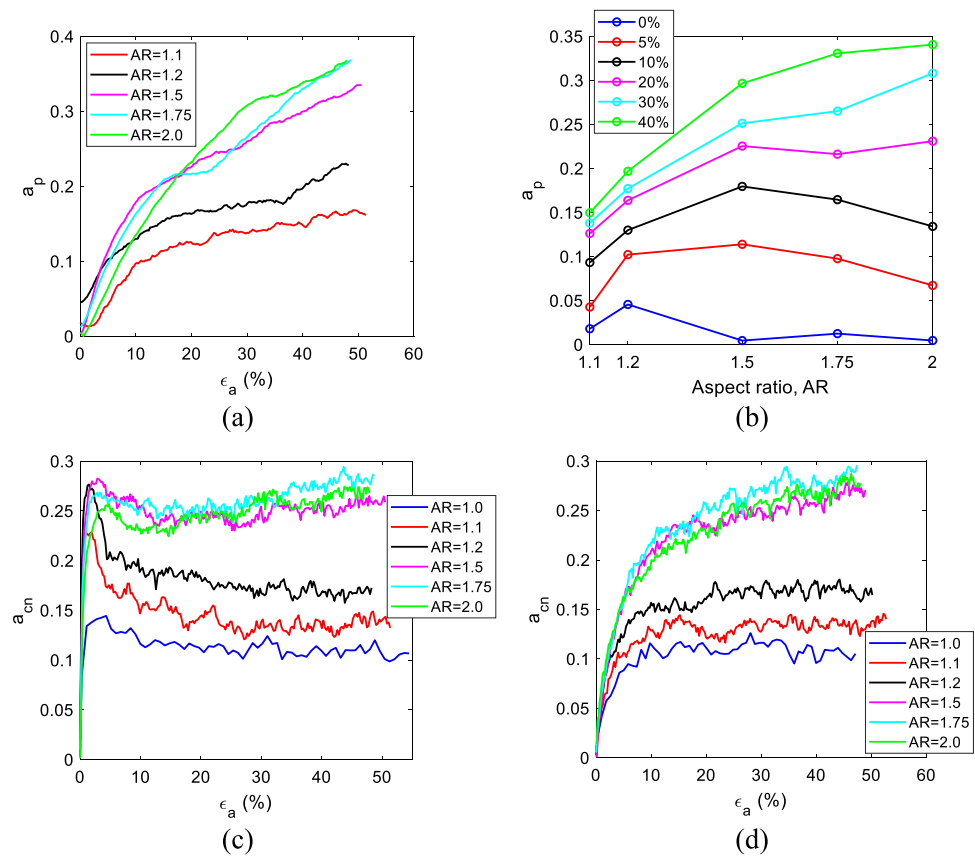


**Fig. 13** Effect of  $AR$  on (a) the evolution of particle orientation anisotropy,  $a_p$ , during shearing (b) particle orientation anisotropy at different shearing stages for dense ( $\mu_{prep} = 0.01$ ) samples having  $C_u = 1.2$ . Effect of  $AR$  on the evolution of contact normal anisotropy,  $a_{cn}$ , during shearing for (c) dense ( $\mu_{prep} = 0.01$ ) (d) loose ( $\mu_{prep} = 0.3$ ) samples having  $C_u = 1.2$



to an increase in the rotation limiting interlock within their particles [10, 13, 20, 21, 26, 33, 54, 66].

By analysing the rate of particle rotation,  $\frac{|d(\text{meanrotation})|}{d\epsilon_a}$ , exhibited by the granular assemblies during shearing, we found that  $\frac{|d(\text{meanrotation})|}{d\epsilon_a}$  for the initially dense samples ( $\mu_{prep} = 0.01$ ) was characterised by a peak which decreased as the particle  $AR$  increased (Fig. 16c). The  $\frac{|d(\text{meanrotation})|}{d\epsilon_a}$  for the initially loose samples declined until a plateau was reached

at large strains, without any noticeable peak (Fig. 16d). At  $\epsilon_a > 20\%$ , the  $\frac{|d(\text{meanrotation})|}{d\epsilon_a}$  became independent of particle  $AR$ .

The peak in the rate of particle rotation obtained for the dense assemblies decreased as the particle  $AR$  increased. The data presented here indicates that the dilatancy and loss of contacts associated with dense assemblies under drained shearing is accompanied by a significant increase in the rate of particle rotation while the strain softening exhibited by the assemblies is accompanied by a relaxation in the rate of particle rotation.

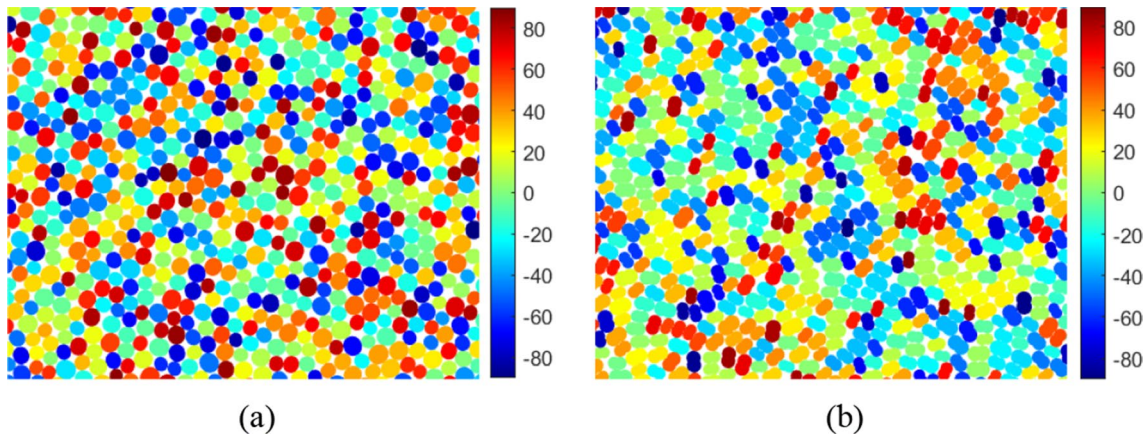
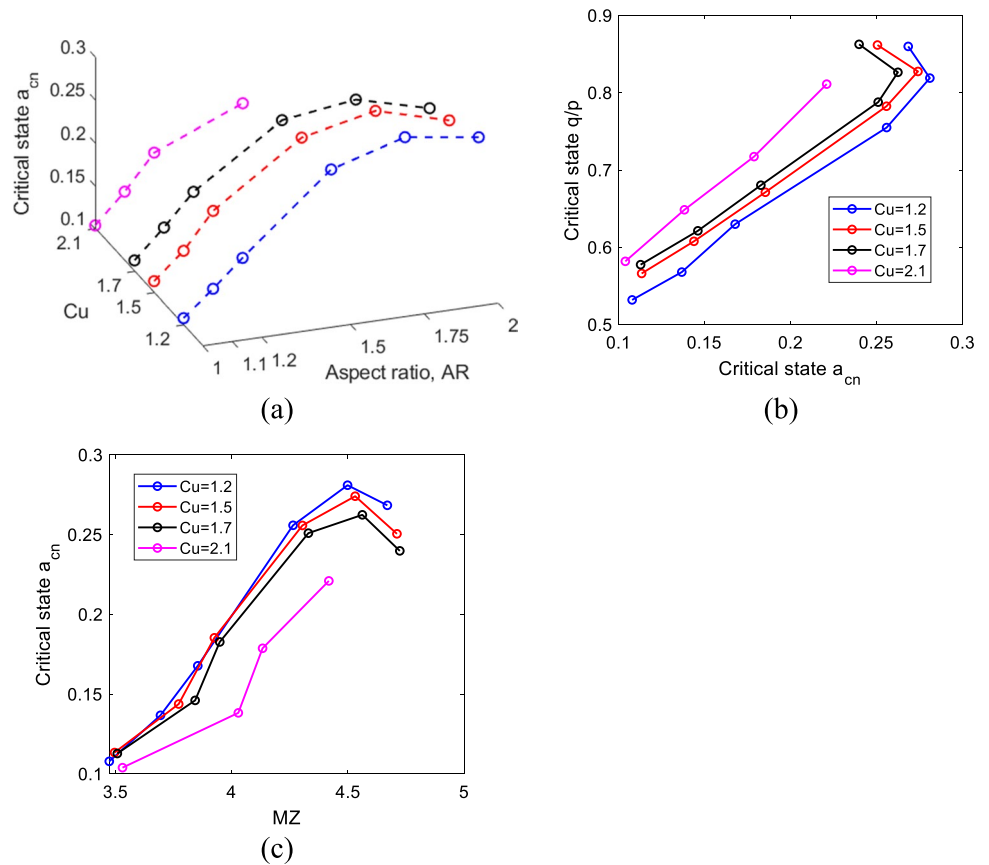


Fig. 14 Colour map of particle orientations for dense samples having  $C_u=1.2$  after 40% of shearing: (a)  $AR=1.1$  (b)  $AR=1.5$

Fig. 15 (a) Effect of  $AR$  on critical state contact normal anisotropy,  $a_{cn}$  (b) Effect of critical state  $MZ$  on critical state  $a_{cn}$  (c) Relationship between critical state  $q/p$  and critical state  $a_{cn}$  for 2D-DEM samples.  $C_u=2.1$  samples which contained 22,477 clump particles were not sheared for  $AR>1.5$



The rate of particle rotation offers a new micro-mechanical data which could be linked to the macroscale characteristics (strength and dilatancy) of granular assemblies.

### 3.7 Particle moment, friction mobilization and the percentage of sliding contacts

Referring to Fig. 17, the particle moment acting on a specified particle is calculated here as:

$$\vec{M}_{cl,k} = \sum_{j=1}^{N_d} \sum_{i=1}^{N_c} (\vec{L}_{ci,j,k} \times \vec{T}_{ci,j,k} + \vec{L}_{ci,j,k} \times \vec{N}_{ci,j,k}) \quad (3)$$

**Fig. 16** Effect of AR and sample density on the mean particle rotation for  $C_u=1.2$  samples during shearing at: (a)  $\epsilon_a = 1\%$  (b)  $\epsilon_a = 40\%$ . Evolution of particle rotation rate during shearing for: (c) dense ( $\mu_{prep} = 0.01$ ) (e) loose ( $\mu_{prep} = 0.3$ ) samples having  $C_u=1.2$  and varying AR

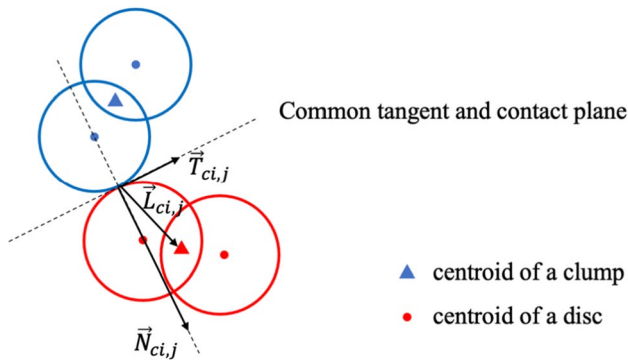
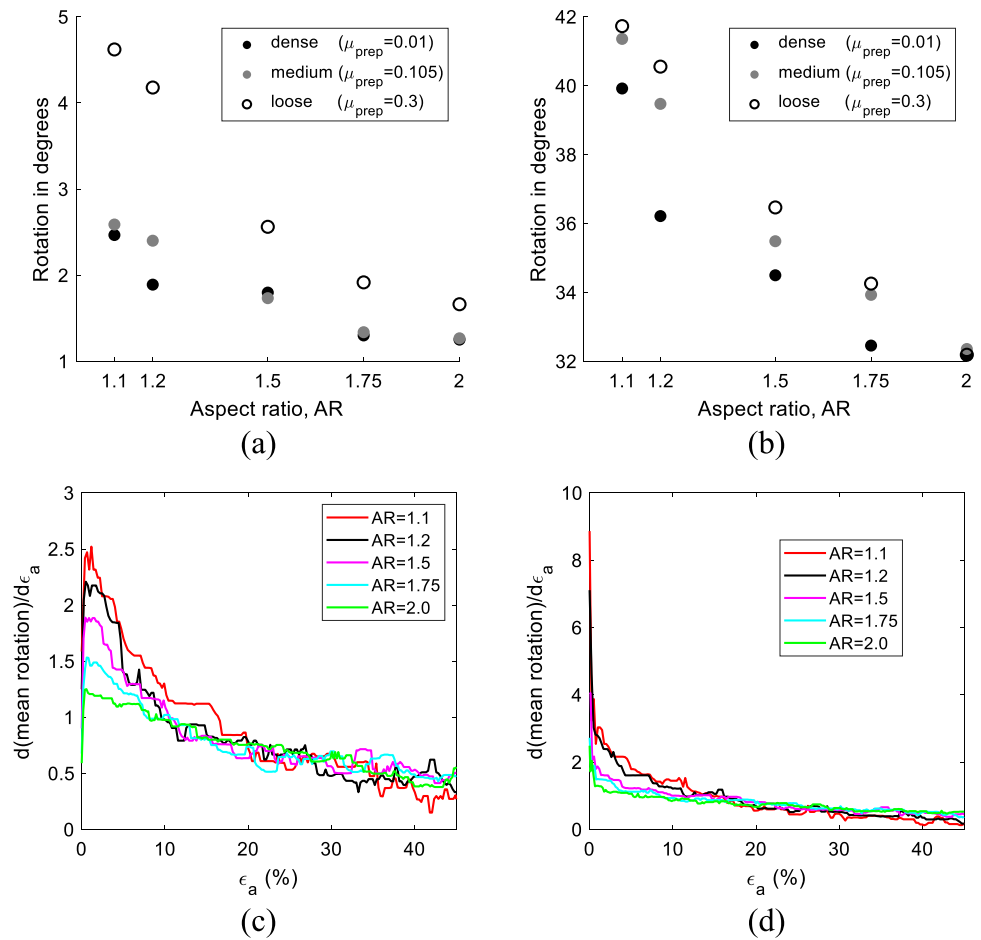


**Fig. 17** Illustration of moments at contacts for the calculation of  $|\sum \vec{M}_T|$  and  $|\sum \vec{M}_N|$

where  $N_d$  is the number of discs in a clump,  $N_c$  is the number of contacts for a disc belonging to the  $k$  clump,  $\vec{L}_{ci,j,k}$  is the contact-centroid branch vector,  $\vec{T}_{ci,j,k}$  is the contact tangential force vector and  $\vec{N}_{ci,j,k}$  is the contact normal force vector. As detailed in Adesina et al. [22], since the simulations

are quasi-static, the particles attained moment equilibrium, therefore, the net moment acting on every particle,  $\vec{M}_{cl,k} \approx 0$ . To quantify the mobilised moment resistance across an assembly, the contribution from the contact shear (normal) force induced moments is isolated, which is indicated by the mean value of the contact shear (normal) force induced moment magnitude:

$$\langle |\vec{M}_T| \rangle = \frac{\sum_{k=1}^{N_p} |\vec{M}_{T,k}|}{N_p} = \frac{\sum_{k=1}^{N_p} |\sum_{j=1}^{N_d} \sum_{i=1}^{N_c} (\vec{L}_{ci,j,k} \times \vec{T}_{ci,j,k})|}{N_p} \tag{4}$$

$$\langle |\vec{M}_N| \rangle = \frac{\sum_{k=1}^{N_p} |\vec{M}_{N,k}|}{N_p} = \frac{\sum_{k=1}^{N_p} |\sum_{j=1}^{N_d} \sum_{i=1}^{N_c} (\vec{L}_{ci,j,k} \times \vec{N}_{ci,j,k})|}{N_p} \tag{5}$$

where  $\langle |\vec{M}_T| \rangle$  and  $\langle |\vec{M}_N| \rangle$  are the isolated mean values of the magnitude of the contact shear and normal force induced moment, respectively.  $N_p$  is the total number of particles in the assembly and  $|\vec{M}_{T,k}|$  and  $|\vec{M}_{N,k}|$  are, respectively,

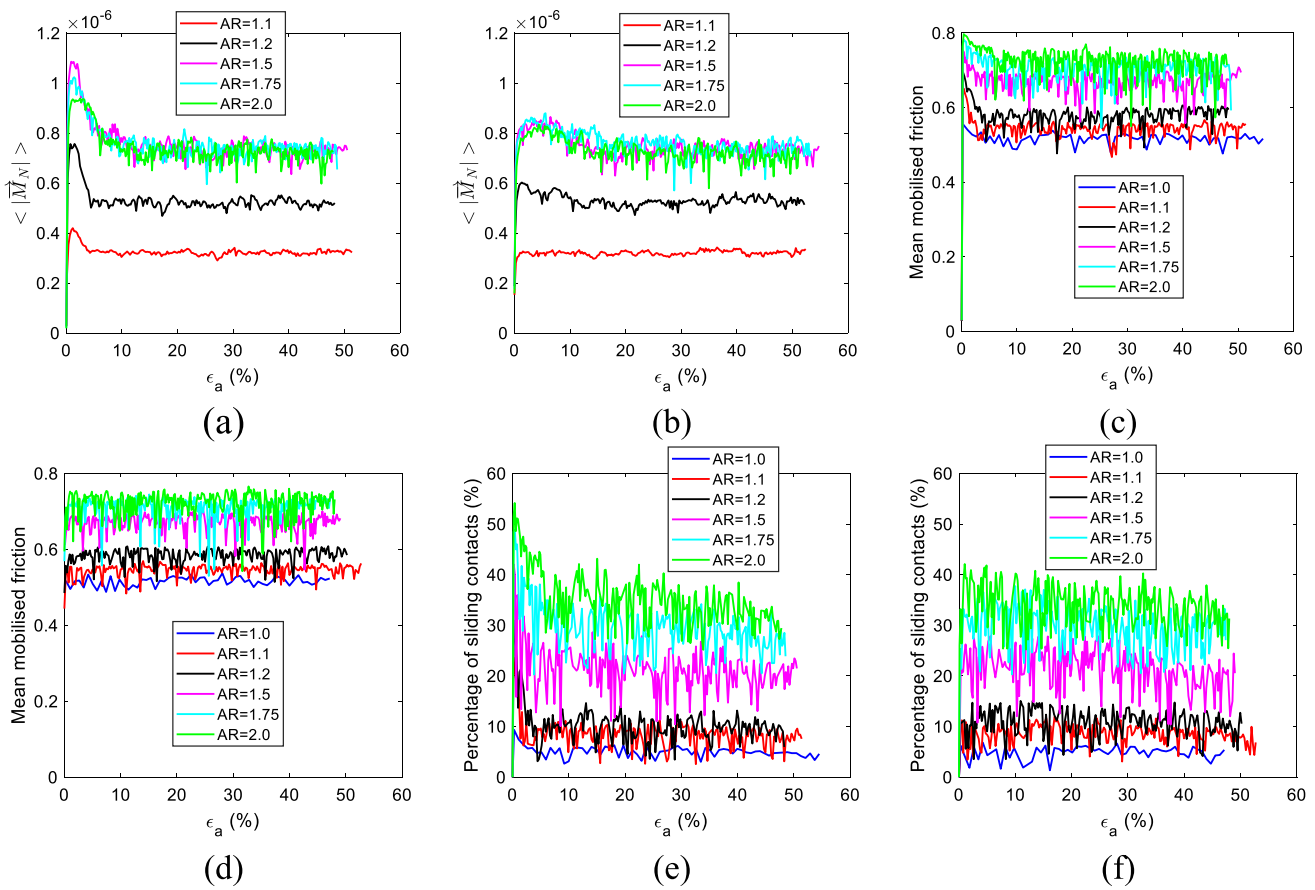


**Fig. 18** Evolution of  $\langle |\overline{M}_N| \rangle$  during shearing for: (a) dense ( $\mu_{prep} = 0.01$ ) (b) loose ( $\mu_{prep} = 0.3$ ) samples having  $C_u = 1.2$  and varying AR. Evolution of mean mobilised friction during shearing for: (c) dense ( $\mu_{prep} = 0.01$ ) (d) loose ( $\mu_{prep} = 0.3$ ) samples having  $C_u$

$= 1.2$  and varying AR. Evolution of percentage of sliding contacts (%) during shearing for: (e) dense ( $\mu_{prep} = 0.01$ ) (f) loose ( $\mu_{prep} = 0.3$ ) samples having  $C_u = 1.2$  and varying AR

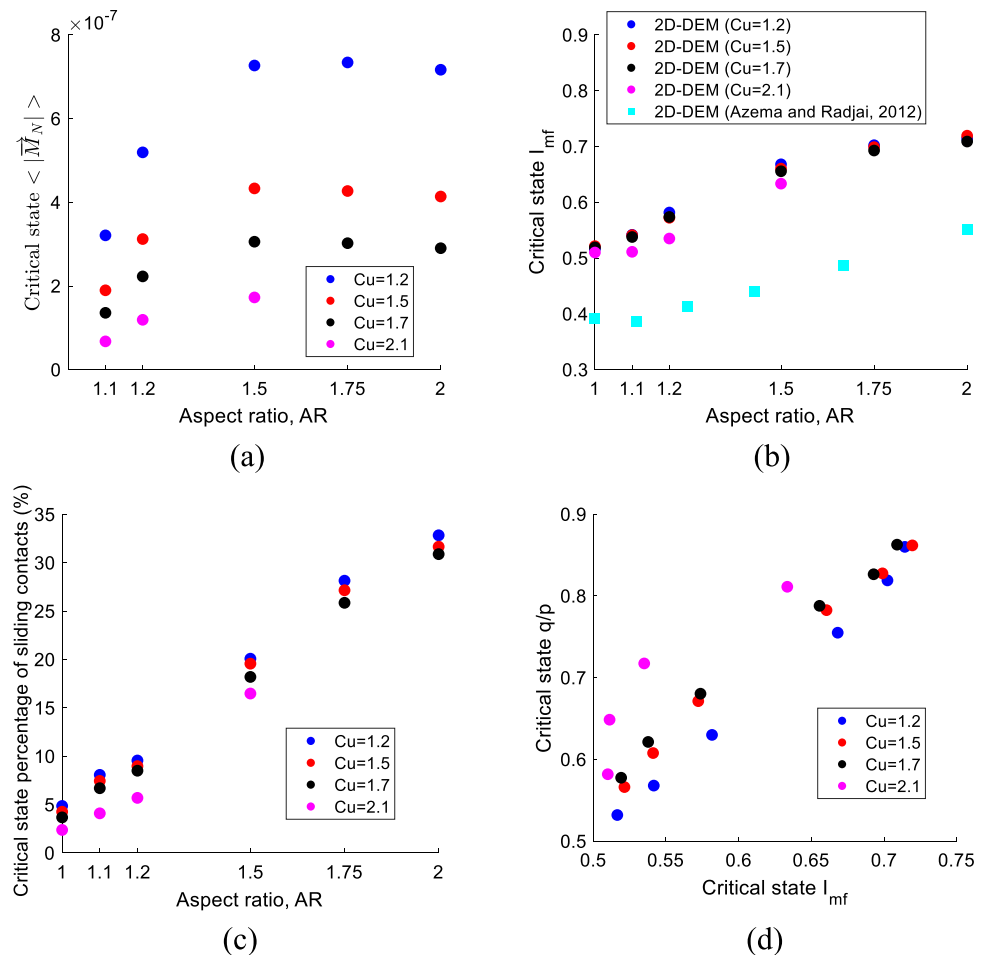
the magnitude of the contact shear and normal force induced moment computed on  $k$  clump.

Figure 18a, b show the evolution of the  $\langle |\overline{M}_N| \rangle$ , for the initially dense ( $\mu_{prep} = 0.01$ ) and the initially loose ( $\mu_{prep} = 0.3$ ) samples having  $C_u = 1.2$ , respectively (Data for  $\langle |\overline{M}_T| \rangle$  are equivalent and so not presented). In a manner similar to the evolution of the  $q/p$  (Fig. 6a, c), the  $\langle |\overline{M}_N| \rangle$  for the initially dense samples increased to a peak and then declined before reaching a plateau at large strains, while the  $\langle |\overline{M}_N| \rangle$  for the initially loose samples increased monotonically to a plateau without a noticeable peak. The same trend was observed in the evolution of the friction mobilisation index,  $I_{mf}$  (Fig. 18c, d), calculated here as  $\langle |F_t|/\mu F_n \rangle$ , following [23, 67]; and in the evolution of the percentage of sliding contacts (Fig. 18e, f), calculated here as the percentage of contacts for which  $|F_t| > 0.9999\mu F_n$ ,

following [45, 68]. The evolution of the proportion of sliding contacts in the granular assemblies of spherical particles with different initial density studied by Guo and Zhao [57] and Gu et al. [68] agrees with the trend reported here. Similar trends were also reported by Ng [18] for assemblies of ellipsoids with varying elongations. The critical state  $\langle |\overline{M}_N| \rangle$  increased as the particle AR increased from  $AR = 1.0$  to  $AR = 1.5$  and then remained fairly constant with further increase in the AR. Also, the critical state  $\langle |\overline{M}_N| \rangle$  decreased with an increase in the  $C_u$  values (Fig. 19a). Both the critical state  $I_{mf}$  (Fig. 19b) and the critical state percentage of sliding contacts (Fig. 19c) increased with an increase in the particle AR, for all  $C_u$  values considered, such that a linear relationship was found between the critical state  $q/p$  and the critical state  $I_{mf}$  for the group of samples at each  $C_u$  value (Fig. 19d).



**Fig. 19** Effect of  $AR$  on (a) critical state  $\langle \overline{M}_{cN} \rangle$  (b) critical state mean mobilised friction (c) critical state percentage of sliding contacts (%) (d) Relationship between critical state  $q/p$  critical state mean mobilised friction,  $I_{mf}$  for 2D-DEM samples



### 4 Concluding remarks

The overall aim of this study was to understand the interplay between three of the most important factors influencing the mechanical behaviour of sand, i.e., the particle shape, particle size distribution and initial sample density. We assessed whether the effect of a factor  $A$  on a mechanical quantity, at a specific instance of a factor  $B$  varies when the instance changes. For example, whether the effect of particle  $AR$  on the peak  $q/p$  at a specific initial density,  $\mu_{prep}$ , is consistent when the initial density is varied. Table 3 summarises this assessment. In addition, we explored the link between the macroscopic characteristics of the assemblies studied and their underlying micromechanical features in order to unravel insights that could help to better understand laboratory data. The following are the conclusions derived from this study:

As shown in Table 3, the effect each of the factors considered in this study has on both the macroscopic and the microscopic characteristics of the granular assemblies studied was not always consistent when other factors were considered. For example, although the peak

$q/p$  decreased as the initial sample density (controlled by the  $\mu_{prep}$ ) decreased for all  $AR$  values considered, the magnitude of the decrease is influenced by the particle  $AR$  (Fig. 7b); similarly, the effect of the  $AR$  on the peak  $q/p$  varied with the  $\mu_{prep}$  value considered (Fig. 7a). This finding establishes the fact that the interplay between the determining factors is important to comprehensively model the behaviour of granular assemblies. Making a generalisation after considering a single factor will only result in a deficient and misleading prediction of the behaviour of granular materials.

An analysis of the micromechanical features could help to shed light on the interdependencies established between the factors studied here. For example, the effect of the particle  $AR$  on the  $\Delta MZ_{ini}$  provides an explanation for why the effect a change in packing density has on the peak strength varies with the  $AR$ .

Our DEM data suggest that the strength-dilatancy relationship is a unique characteristic of granular assemblies. A remarkable linear relationship between strength and dilatancy, similar to that reported in the experimental study on sands by Bolton [61] was established for

**Table 3** Assessment of the interplay between factors

		$\mu_{prep}$	AR	$C_u$
Initial $e$	$\mu_{prep}$	—	✓	✓
	AR	✗	—	✓
	$C_u$	✓	✓	—
Initial MZ	$\mu_{prep}$	—	✗	✓
	AR	✗	—	✓
	$C_u$	✓	✓	—
Peak $q/p$	$\mu_{prep}$	—	✗	✗
	AR	✗	—	✓
	$C_u$	✓	✗	—
Critical state $q/p$	$\mu_{prep}$	—	✓	✓
	AR	—	—	✗
	$C_u$	—	✓	—
$(-d\varepsilon_v/d\varepsilon_a)_{max}$	$\mu_{prep}$	—	✗	✗
	AR	✓	—	✗
	$C_u$	✓	✓	—
Critical state $e$ & Critical state MZ	$\mu_{prep}$	—	✓	✓
	AR	—	—	✓
	$C_u$	—	✓	—
Critical state $a_{cn}$	$\mu_{prep}$	—	✓	✗
	AR	—	—	✗
	$C_u$	—	✓	—
Critical state Mean particle rotation	$\mu_{prep}$	—	✓	✓
	AR	✓	—	✓
	$C_u$	✓	✓	—
Critical state $\langle  \overline{M}_N  \rangle$	$\mu_{prep}$	—	✓	✓
	AR	—	—	✓
	$C_u$	—	✓	—
Critical state $I_{mf}$	$\mu_{prep}$	—	✓	✓
	AR	—	—	✗
	$C_u$	—	✓	—

Note: ✓ means the effect of a factor (e.g.  $\mu_{prep}$ ) on a quantity (e.g. initial  $e$ ) at a specific instance of another factor (e.g.  $C_u$ ) is consistent when the instance changes. In other words, the effect of  $\mu_{prep}$  on the initial  $e$  is consistent for all  $C_u$  considered. ✗ means the effect of a factor (e.g. AR) on a quantity (e.g. peak  $q/p$ ) is not consistent when another factor (e.g.  $\mu_{prep}$ ) is varied. — means a factor (e.g.  $\mu_{prep}$ ) has NO effect on a quantity (e.g. critical state  $q/p$ ) either when the same factor ( $\mu_{prep}$ ) is considered or when another factor (e.g.  $C_u$ ) is varied

the assemblies of varying particle shapes and gradings in this DEM study.

Our DEM data show that the percentage of contact loss during shearing correlates strongly with the degree of strain softening exhibited by the granular assemblies. In contrast to the finding in the experimental study by Amirrahmat et al. [54] which suggested that particle AR did not seem to influence the percentage of contact loss during shearing, we establish here that the per-

centage of contact loss indeed depends on AR and correlates strongly with the dilatancy of the samples. By establishing a relationship between the peak dilatancy and the contact loss during shearing by the assemblies studied here, we provide an evidence for the claim that dilatancy in dense sands is accompanied by the loss of contacts.

In agreement with earlier studies on the behaviour of granular materials, we confirmed that particle shape influences the fabric anisotropy of granular assemblies and this ultimately determines the strength mobilised by the assemblies. Also, the strength mobilised by assemblies of non-spherical particles could be linked with the rate of particle rotation within the assemblies. We found that prior to the critical state, the rate of rotation decreased with an increase in the particle AR during shearing. The rate of particle rotation determined in this study provides a micromechanical data that is not common in previous DEM studies where only the magnitude of particle rotation has been linked with shear strength.

We acknowledge that the out-of-plane system response ignored in our 2-D simulations may not accurately represent the contact interactions and volumetric response of 3-D granular samples. Nevertheless, by comparing our 2-D DEM data with the data from experimental and 3-D DEM studies including data from similar studies in 2-D (as shown in Figs. 4a, b, 7a, d, 8d and 19b), we demonstrate the trends found in our study agrees well with the observations in 3-D studies of granular assemblies subjected to drained shearing. In order to further substantiate the relevance of the observations made here to the behaviour of sand, we recommend that a similar study involving three-dimensional representation of real sand particles should be conducted in the future.

**Acknowledgements** All simulations were conducted using the high-performance computing (HPC) facilities at Imperial College London. Peter Adesina’s doctoral research is sponsored by the Commonwealth Scholarship Commission, UK and Imperial College London. Code development work carried out by Tokio Morimoto, Masahide Otsubo, and Kevin Hanley enabled this research.

**Conflict of interest** The authors declare that they have no known competing financial interests or personal relationships that could have appeared to influence the work reported in this paper.

**Open Access** This article is licensed under a Creative Commons Attribution 4.0 International License, which permits use, sharing, adaptation, distribution and reproduction in any medium or format, as long as you give appropriate credit to the original author(s) and the source, provide a link to the Creative Commons licence, and indicate if changes were made. The images or other third party material in this article are included in the article’s Creative Commons licence, unless indicated

otherwise in a credit line to the material. If material is not included in the article's Creative Commons licence and your intended use is not permitted by statutory regulation or exceeds the permitted use, you will need to obtain permission directly from the copyright holder. To view a copy of this licence, visit <http://creativecommons.org/licenses/by/4.0/>.

## References

- Altuhafi, F., O'Sullivan, C., Cavarretta, I.: Analysis of an image-based method to quantify the size and shape of sand particles. *J. Geotech. Geoenvironmental Eng.* **139**(8), 1290–1307 (2013)
- Altuhafi, F.N., Coop, M.R., Georgiannou, V.N.: Effect of particle shape on the mechanical behavior of natural sands. *J. Geotech. Geoenvironmental Eng.* **142**(12), 04016071 (2016)
- Holubec, I., D'Appolonia, E.: Effect of particle shape on the engineering properties of granular soils. *Eval. Relat. Density Its Role Geotech. Proj. Invol. Cohesionless Soils, ASTM STP 523*, 304–318 (1973)
- Santamarina JC, Cho GC. Soil behaviour: The role of particle shape. In: *Advances in Geotechnical Engineering: The Skempton Conference – Proceedings of a Three Day Conference on Advances in Geotechnical Engineering*, organised by the Institution of Civil Engineers. 2004. p. 604–17.
- Sezer, A., Altun, S., Göktepe, B.A.: Relationships between shape characteristics and shear strength of sands. *Soils Found.* **51**(5), 857–871 (2011)
- Ting, J.M., Meachum, L., Rowell, J.D.: Effect of particle shape on the strength and deformation mechanisms of ellipse-shaped granular assemblages. *Eng. Comput.* **12**(2), 99–108 (1995)
- Cundall, P.A., Strack, O.D.L.: A discrete numerical model for granular assemblies. *Geotechnique* **30**(3), 331–336 (1979)
- Azéma E, Radjai F. Stress-strain behavior and geometrical properties of packings of elongated particles. *Phys. Rev. E Stat Nonlinear Soft Matter Phys.* 2010;81(5).
- Gong J, Nie Z, Zhu Y, Liang Z, Wang X. Exploring the effects of particle shape and content of fines on the shear behavior of sand-fines mixtures via the DEM. *Comput. Geotech.* [Internet]. 2019;106(November 2018):161–76. Available from: <https://doi.org/10.1016/j.compgeo.2018.10.021>
- Härtl J, Ooi JY. Numerical investigation of particle shape and particle friction on limiting bulk friction in direct shear tests and comparison with experiments. *Powder Technol.* [Internet]. 2011;212(1):231–9. Available from: <https://doi.org/10.1016/j.powtec.2011.05.022>
- Matsushima. Effect of irregular grain shape on quasi-static shear behavior of granular assembly. *Powders Grains 2005 - Proc 5th Int Conf Micromechanics Granul Media.* 2005;2(July):1319–23.
- Nie Z, Fang C, Gong J, Liang Z. DEM study on the effect of roundness on the shear behaviour of granular materials. *Comput. Geotech.* 2020;121(September 2019).
- Peña, A.A., García-Rojo, R., Herrmann, H.J.: Influence of particle shape on sheared dense granular media. *Granul. Matter* **9**(3–4), 279–291 (2007)
- Estrada, N.: Effects of grain size distribution on the packing fraction and shear strength of frictionless disk packings. *Phys. Rev. E* **062903**(94), 1–7 (2016)
- He, J., Liu, F., Deng, G., Fu, P.: Relationships between gradation and deformation behavior of dense granular materials: role of high-order gradation characteristics. *Int. J. Numer. Anal Methods Geomech.* **45**(12), 1791–1808 (2021)
- Nguyen, D.H., Azéma, E., Sornay, P., Radjai, F.: Effects of shape and size polydispersity on strength properties of granular materials. *Phys. Rev. E* **91**(3), 1–9 (2015)
- Voivret, C., Radjai, F., Delenne, J.Y., El Youssoufi, M.S.: Multiscale force networks in highly polydisperse granular media. *Phys. Rev. Lett.* **178001**(102), 1–5 (2009)
- Ng, T.T.: Triaxial test simulations with discrete element method and hydrostatic boundaries. *J. Eng. Mech.* **130**(10), 1188–1194 (2004)
- Matsushima, T., Chang, C.S.: Quantitative evaluation of the effect of irregularly shaped particles in sheared granular assemblies. *Granul. Matter* **13**(3), 269–276 (2011)
- Salot, C., Gotteland, P., Villard, P.: Influence of relative density on granular materials behavior: DEM simulations of triaxial tests. *Granul. Matter* **11**(4), 221–236 (2009)
- Abedi, S., Mirghasemi, A.A.: Particle shape consideration in numerical simulation of assemblies of irregularly shaped particles. *Particuology*. **9**(4), 387–397 (2011)
- Adesina PA, O'Sullivan C, Wang T. DEM study on the effect of particle shape on the shear behaviour of granular materials. *Comput. Part Mech.* 2023 (Accepted).
- Azéma, E., Radjai, F.: Force chains and contact network topology in sheared packings of elongated particles. *Phys. Rev. E Stat. Nonlinear Soft Matter Phys.* **85**(3), 1–12 (2012)
- Fazelpour, F., Tang, Z., Daniels, K.E.: The effect of grain shape and material on the nonlocal rheology of dense granular flows. *Soft Matter* **18**(7), 1435–1442 (2022)
- Jerves, A.X., Kawamoto, R.Y., Andrade, J.E.: Effects of grain morphology on critical state: A computational analysis. *Acta Geotech.* **11**(3), 493–503 (2016)
- Maeda, K., Sakai, H., Kondo, A., Yamaguchi, T., Fukuma, M., Nukudani, E.: Stress-chain based micromechanics of sand with grain shape effect. *Granul. Matter* **12**(5), 499–505 (2010)
- Marteau, E., Andrade, J.E.: An experimental study of the effect of particle shape on force transmission and mobilized strength of granular materials. *J. Appl. Mech.* **88**(11), 1–10 (2021)
- Wei, D., Wang, J., Nie, J., Zhou, B.: Generation of realistic sand particles with fractal nature using an improved spherical harmonic analysis. *Comput. Geotech.* **104**(August), 1–12 (2018)
- Wang S, Marmysh D, Ji S. Construction of irregular particles with superquadric equation in DEM. *Theor. Appl. Mech. Lett.* [Internet]. 2020;10(2):68–73. Available from: <https://doi.org/10.1016/j.taml.2020.01.021>
- Hogue, C.: Shape representation and contact detection for discrete element simulations of arbitrary geometries. *Eng. Comput.* **15**(2–3), 374–390 (1998)
- Kafashan J, Wiącek J, Abd Rahman N, Gan J. Two-dimensional particle shapes modelling for DEM simulations in engineering: a review. *Granul. Matter.* [Internet]. 2019;21(3):1–19. Available from: <https://doi.org/10.1007/s10035-019-0935-1>
- Kodicherla SPK, Gong G, Yang ZX, Krabbenhoft K, Fan L, Moy CKS, et al. The influence of particle elongations on direct shear behaviour of granular materials using DEM. *Granul. Matter.* [Internet]. 2019;21(4):1–12. Available from: <https://doi.org/10.1007/s10035-019-0947-x>
- Tian J, Liu E, Jiang L, Jiang X, Sun Y, Xu R. Influence of particle shape on the microstructure evolution and the mechanical properties of granular materials. *Comptes Rendus Mec* [Internet]. 2018;346(6):460–76. Available from: <https://doi.org/10.1016/j.crme.2018.03.006>
- Xie, Y.H., Yang, Z.X., Barreto, D.: The influence of particles' aspect ratio on the shear behaviour of granular materials. *Springer Proc. Phys.* **188**, 253–264 (2017)

35. Yang Y, Wang JF, Cheng YM. Quantified evaluation of particle shape effects from micro-to-macro scales for non-convex grains. *Particuology* [Internet]. 2016;25:23–35. Available from: <https://doi.org/10.1016/j.partic.2015.01.008>
36. Molina, S.L., Azema, E., Estrada, N., Fityus, S., Simmons, J., Lizcano, A.: Impact of grading on steady-state strength. *Geotech. Lett.* **9**(4), 328–333 (2019)
37. Li G, Liu Y jing, Dano C, Hicher P yves, Li G, Liu Y jing, et al. Grading-dependent behavior of granular materials: from discrete to continuous modeling. *J. Eng. Mech.* 2014;141(6):0–15.
38. Liu, D., O’Sullivan, C., Carraro, J.A.H.: Influence of particle size distribution on the proportion of stress-transmitting particles and implications for measures of soil state. *J. Geotech. Geoenvironmental Eng.* **147**(3), 04020182 (2021)
39. Adesina P, O’Sullivan C, Morimoto T, Otsubo M. Determining a representative element volume for DEM simulations of samples with non-circular particles. *Particuology* [Internet]. 2022;68:29–43. Available from: <https://doi.org/10.1016/j.partic.2021.10.007>
40. Azéma, E., Linero, S., Estrada, N., Lizcano, A.: Shear strength and microstructure of polydisperse packings : The effect of size span and shape of particle size distribution. *Phys. Rev. E* **96**(022902), 1–10 (2017)
41. Morimoto T, Otsubo M, Koseki J. Microscopic investigation into liquefaction resistance of pre-sheared sand: effects of particle shape and initial anisotropy. *Soils Found* [Internet]. 2021;61(2):335–51. Available from: <https://doi.org/10.1016/j.sandf.2020.12.008>
42. Nguyen TD, Plimpton SJ. Aspherical particle models for molecular dynamics simulation. *Comput. Phys. Commun.* [Internet]. 2019;243:12–24. Available from: <https://doi.org/10.1016/j.cpc.2019.05.010>
43. Plimpton, S.: Fast Parallel Algorithms for Short-Range Molecular Dynamics. *J. Comput. Phys.* **117**(1), 1–19 (1995)
44. da Cruz F, Emam S, Prochnow M, Roux J noël, Chevoir F. Rheophysics of dense granular materials: discrete simulation of plane shear flows. *Phys. Rev.* 2005;72(February):1–17.
45. Gong, J., Liu, J.: Effect of aspect ratio on triaxial compression of multi-sphere ellipsoid assemblies simulated using a discrete element method. *Particuology*. **32**, 49–62 (2017)
46. Guises, R., Xiang, J., Latham, J.P., Munjiza, A.: Granular packing: Numerical simulation and the characterisation of the effect of particle shape. *Granul. Matter* **11**(5), 281–292 (2009)
47. Youd TL. Factors controlling maximum and minimum densities of sands. *ASTM Spec. Tech. Publ.* 1973;(October):98–112.
48. Shire T. Micro-scale Modelling of Granular Filters. Thesis submitted to the Department of Civil and Engineering Civil and Environmental Engineering, Imperial College, London, United Kingdom. 2014.
49. Thornton, C.: Numerical simulations of deviatoric shear deformation of granular media. *Geotechnique* **50**(1), 43–53 (2000)
50. Donev A, Cisse I, Sachs D, Vario EA., Stillinger FH, Connelly R, et al. Improving the density of jammed disordered packings using ellipsoids. *Science* (80- ) [Internet]. 2004;303(990):4. Available from: [papers://1a426bdf-ecfe-4153-8e8c-47052d9a4c31/Paper/p115](https://papers://1a426bdf-ecfe-4153-8e8c-47052d9a4c31/Paper/p115)
51. Rothenburg, L., Kruyt, N.P.: Critical state and evolution of coordination number in simulated granular materials. *Int. J. Solids Struct.* **41**(21), 5763–5774 (2004)
52. Craig RF. *Craig’s Soil Mechanics*. Spon Press, Taylor & Francis Group, London and New York. 2004. 102–105 p.
53. Jefferies M, Been K. *Soil liquefaction: a critical state approach*. Vol. 2. 2016. 35–100 p.
54. Amirrahmat, S., Druckrey, A.M., Alshibli, K.A., Al-Raoush, R.I.: Micro shear bands: precursor for strain localization in sheared granular materials. *J. Geotech. Geoenvironmental Eng.* **145**(2), 1–18 (2019)
55. Been, K., Jefferies, M.G.: A state parameter for sands. *Geotechnique* **35**(2), 99–112 (1986)
56. Zhu, H., Nicot, F., Darve, F.: Meso-structure evolution in a 2D granular material during biaxial loading. *Granul. Matter* **18**(1), 1–12 (2016)
57. Guo N, Zhao J. The signature of shear-induced anisotropy in granular media. *Comput. Geotech.* [Internet]. 2013;47:1–15. Available from: <https://doi.org/10.1016/j.compgeo.2012.07.002>
58. Deng, N., Wautier, A., Tordesillas, A., Thiery, Y., Yin, Z.Y., Hicher, P.Y., et al.: Lifespan dynamics of cluster conformations in stationary regimes in granular materials. *Phys. Rev. E* **105**(1), 1–15 (2022)
59. Xiao, Y., Long, L., Matthew Evans, T., Zhou, H., Liu, H., Stuedlein, A.W.: Effect of particle shape on stress-dilatancy responses of medium-dense sands. *J. Geotech. Geoenvironmental Eng.* **145**(2), 04018105 (2019)
60. Jiang MD, Yang ZX, Barreto D, Xie YH. The influence of particle-size distribution on critical state behavior of spherical and non-spherical particle assemblies. *Granul. Matter.* [Internet]. 2018;20(4):1–15. Available from: <https://doi.org/10.1007/s10035-018-0850-x>
61. Bolton, M.D.: The strength and dilatancy of sands. *Geotechnique* **36**(1), 65–78 (1986)
62. Rothenburg, L., Bathurst, R.J.: Micromechanical features of granular assemblies with planar elliptical particles. *Geotechnique* **42**(1), 79–95 (1992)
63. Zhao S, Evans TM, Zhou X. Shear-induced anisotropy of granular materials with rolling resistance and particle shape effects. *Int. J. Solids Struct.* [Internet]. 2018;150:268–81. Available from: <https://doi.org/10.1016/j.ijsolstr.2018.06.024>
64. Cho, G.C., Dodds, J., Santamarina, J.C.: Particle shape effects on packing density, stiffness, and strength: natural and crushed sands. *J. Geotech. Geoenvironmental Eng.* **132**(5), 591–602 (2006)
65. Satake M. Fabric tensor in granular materials. In: PA Vermeer & HJ Luger (eds) *IUTAM Symposium on Deformations and Failure of Granular Materials 1982* Rotterdam: Balkema. 1982. p. 63–8.
66. Thomas, P.A., Bray, J.D.: Capturing nonspherical shape of granular media with disk clusters. *J. Geotech. Geoenvironmental Eng.* **125**(3), 169–178 (1999)
67. Majmudar, T.S., Behringer, R.P.: Contact force measurements and stress-induced anisotropy in granular materials. *Nature* **435**(7045), 1079–1082 (2005)
68. Gu, X., Huang, M., Qian, J.: DEM investigation on the evolution of microstructure in granular soils under shearing. *Granul. Matter* **16**(1), 91–106 (2014)

**Publisher’s Note** Springer Nature remains neutral with regard to jurisdictional claims in published maps and institutional affiliations.